Redox Properties of Ferrocenyl Ene-diynyl Bridged Cp*(dppe)M-C≡C-1,4-(C_6H_4) Complexes

Rim Makhoul,[‖] Josef B. G. Gluyas,[§] Kevin B. Vincent,[†] Hiba Sahnoune[‡,‖] Jean-François Halet,*[,‖] Paul J. Low,*[,§] Jean-René Hamon,[‖] and Claude Lapinte*[,‖]

[‖] Université Rennes, CNRS, ISCR (Institut des Sciences Chimiques de Rennes) - UMR 6226, F-35000 Rennes, France

[§]School of Molecular Sciences, University of Western Australia, 35 Stirling Highway, Crawley, Western Australia, 6009, Australia

[†]Department of Chemistry, Durham University, South Rd, Durham, DH1 3LE, UK

[‡]Département de Chimie, Faculté des Sciences, Université M'Hamed Bougara, Boumerdès, Algeria

Table of Contents Graphic

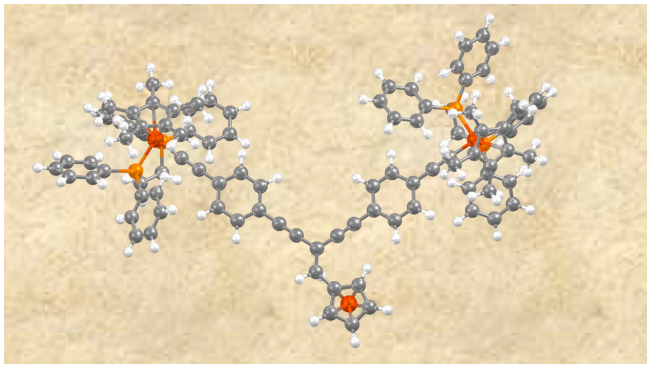

ABSTRACT: The complexes FcCH=C{1,4-C≡C-C_6H_4-C≡CM(dppe)Cp*}$_2$ (Fc = ferrocenyl (FeCp(η-C_5H_4-); M = Fe (**1**), Ru (**2**)) were prepared from FcCH=C{1,4-C≡C-C_6H_4-C≡C$SiMe_3$}$_2$ (**3**) via a desilylation / metallation protocol in good (**2**, 65%) to excellent (**1**, 97%) yield. The iron compound **1** could also be prepared in stepwise fashion by desilylation of **3** to give FcCH=C{1,4-C≡C-C_6H_4-C≡CH}$_2$ (**4**), reaction with FeCl(dppe)Cp* to give the vinylidene complex FcCH=C{1,4-C≡C-C_6H_4-CH=C=Fe(dppe)Cp*}$_2$]$(PF_6)_2$ (**5(PF$_6$)$_2$**, 65%), and deprotonation. The cyclic voltammograms of **1** and **2** are characterized by an initial oxidation wave resulting from the overlap of two closely spaced oxidation processes, the potentials of which are sensitive to the identity of M, and a subsequent, 1-electron oxidation wave. Thus, whilst the dications $\mathbf{1}^{2+}$ and $\mathbf{2}^{2+}$ could be prepared by oxidation with 2 equiv. ferrocenium hexafluorophosphate and isolated as the PF_6^- salts **1(PF$_6$)$_2$** and **2(PF$_6$)$_2$** at low temperature, the monocations $\mathbf{1}^+$ and $\mathbf{2}^+$ could only be detected and studied as comproportionated mixtures of **1**, **1(PF$_6$)**, **1(PF$_6$)$_2$** and **2**, **2(PF$_6$)**, **2(PF$_6$)$_2$**. A combination of EPR spectroscopy, IR and NIR spectroelectrochemistry and DFT quantum chemical calculations reveal subtle distinctions in the electronic structures of **1(PF$_6$)$_n$** and **2(PF$_6$)$_n$** (n = 0, 1, 2). The HOMOs of **1** and **2** are more heavily distributed over the metal-diethynylbenzene arm *trans* to the ferrocenyl moiety. Whilst 1-electron oxidation of **1** gives **1(PF$_6$)** in which the spin density is similarly distributed along the branch of the molecule *trans* to the ferrocenyl group, the spin density in **2(PF$_6$)** is more extensively, but not fully, delocalized. Further analysis of the ESR, NIR and IR spectra reveal that charges are essentially localized in **1(PF$_6$)** and **1(PF$_6$)$_2$**, on the IR timescale, but ground-state exchange between the Fe(dppe)Cp* moieties can take place via the ferrocenyl

moiety on the slower ESR timescale. For **2(PF$_6$)** and **2(PF$_6$)$_2$**, optical charge transfer processes between the ferrocenyl moiety and the organometallic branches can also be observed, consistent with the increased coupling between the Ru(dppe)Cp* and Fc moieties that are linked by a linear conjugation pathway through the bridging-ligand backbone.

INTRODUCTION

In recent years, the search for more highly functional systems that access unusual electronic structures and permit greater control and manipulation of intramolecular charge transfer processes has seen attention also turned to systems bearing cross-conjugated bridging moieties,[1-4] including mixed-valence derivatives.[5-8] These studies in turn form part of a larger range of investigations that address more general questions about the ability to tune the electrical behavior of cross-conjugated systems through the manipulation of quantum interference features.[9-13]

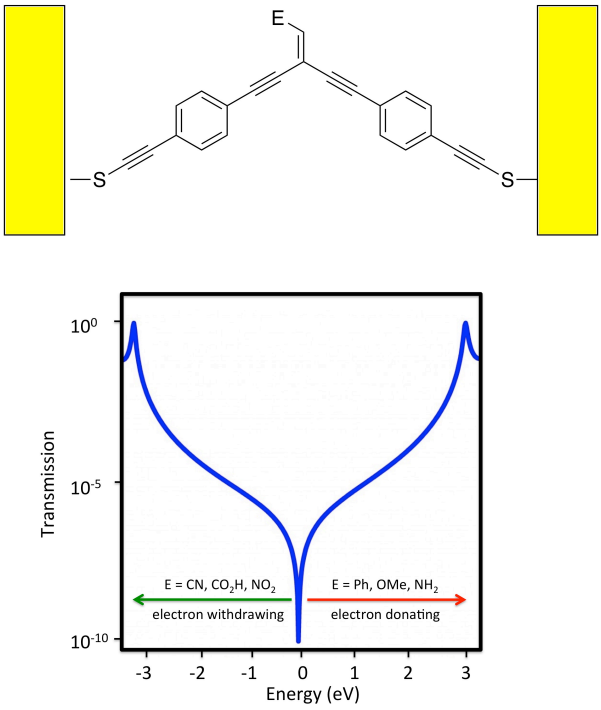

Figure 1. A cartoon sketch of an anti-resonance arising from QI through a molecular junction formed from a cross-conjugated *gem*-diethynylethene, based on the work of Andrews et al..[14] The energy of the anti-resonance is sensitive to the chemical structure of the pendent group, E.

Quantum interference (QI) arises from the interaction of the de Broglie waves of electrons traversing a molecular system with the accessible molecular energy levels.[15] The sum of these interactions can be constructive, giving rise to resonances and effective electron transport (e.g. through a *para*-substituted benzene), or destructive, giving rise to anti-resonances and heavily restricted electron transport (e.g. through a *meta*-substituted benzene).[16-17] It has been proposed that the energy of a QI anti-resonance can not only be influenced by the structure of the molecular backbone such as linear vs cross-conjugated scaffolds or introduction of pendant groups,[9, 18-20] but can also be tuned through the

introduction of electron-donating or withdrawing groups to the molecular backbone (Figure 1).[21] As QI effects are persistent in even quite large molecular systems,[14] the opportunity to explore chemical control over QI effects is an exciting area of contemporary chemistry.[22-23]

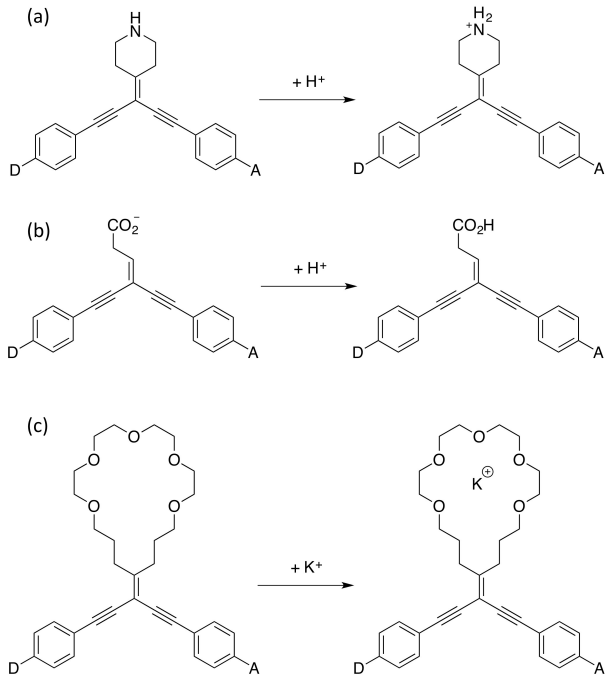

Figure 2. The chemically gated QI systems proposed by Grozema and colleagues.[24]

With these concepts in mind, Grozema's proposal of a chemically gated QI-based molecular transistor provided a fascinating structural model through which to explore and modulate molecule-mediated charge transfer processes between a donor and an acceptor (Figure 2).[24] As noted above, the effects of QI can be modulated through the introduction of electron donating or withdrawing groups pendant to the electron transfer channel. The Grozema system proposes the protonation of a pendant amine or caboxylate group or

alkali metal ion coordination to a pendant crown to change the electrostatic potential of the pendent group to chemically 'gate' the interference patterns of the propagating electron waves between the donor and acceptor sites.

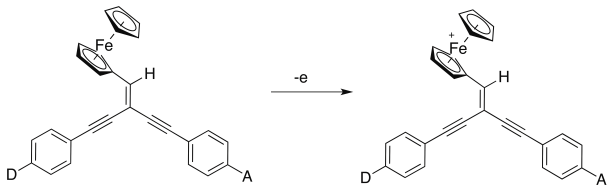

Figure 3. An electrochemically gated analogue of Grozema's QI transistor.

In seeking to extend these concepts, our attention has been drawn to electrochemically-gated systems, with a redox-active pendant introduced to a general donor-bridge-acceptor structure. By tuning the formal redox state of the gate, a change in the QI patterns between the donor and acceptor should be introduced (Figure 3). We have chosen to base our design strategy around mixed-valence compounds in which the donor and acceptor differ only through their formal oxidation state.[25-28] Indeed, in recent times there has been a resurgence of interest in mixed-valence models of intramolecular charge-transfer processes, with the development of theoretical descriptions and spectroscopic analysis of the charge-transfer event[29] to the development of novel optoelectronic materials and the design of molecular electronic components.[30]

Some of the present authors have explored aspects, including mixed-valence characteristics, of cross-conjugated 1,1-bis(alkynyl)-2-ferrocenylethene derivatives (**A**),[31] including 1,1-bis(ferocenylalkynyl)-2-ferrocenylethene (**B**)[32] and

tetrakis(ferrocenylethynyl)ethene (**C**)[33] (Chart 1). However, efforts to incorporate the half-sandwich building blocks M(PP)Cp', which have been so successful in exploring other aspects of organometallic mixed-valency when linked through linearly conjugated all-carbon and carbon-rich bridging ligands,[34-40] within the cross-conjugated 1,1-bis(alkynyl)-2-ferrocenylethene framework through desilylation-metallation reactions of 1,1-bis(trimethylsilylethynyl)-2-ferrocenylethene (Chart 1, **A**, R = $SiMe_3$) or via vinylidenes formed from 1,1-bis(ethynyl)-2-ferrocenylethene (Chart 1, **A**, R = H) have so far proved fruitless.[32]

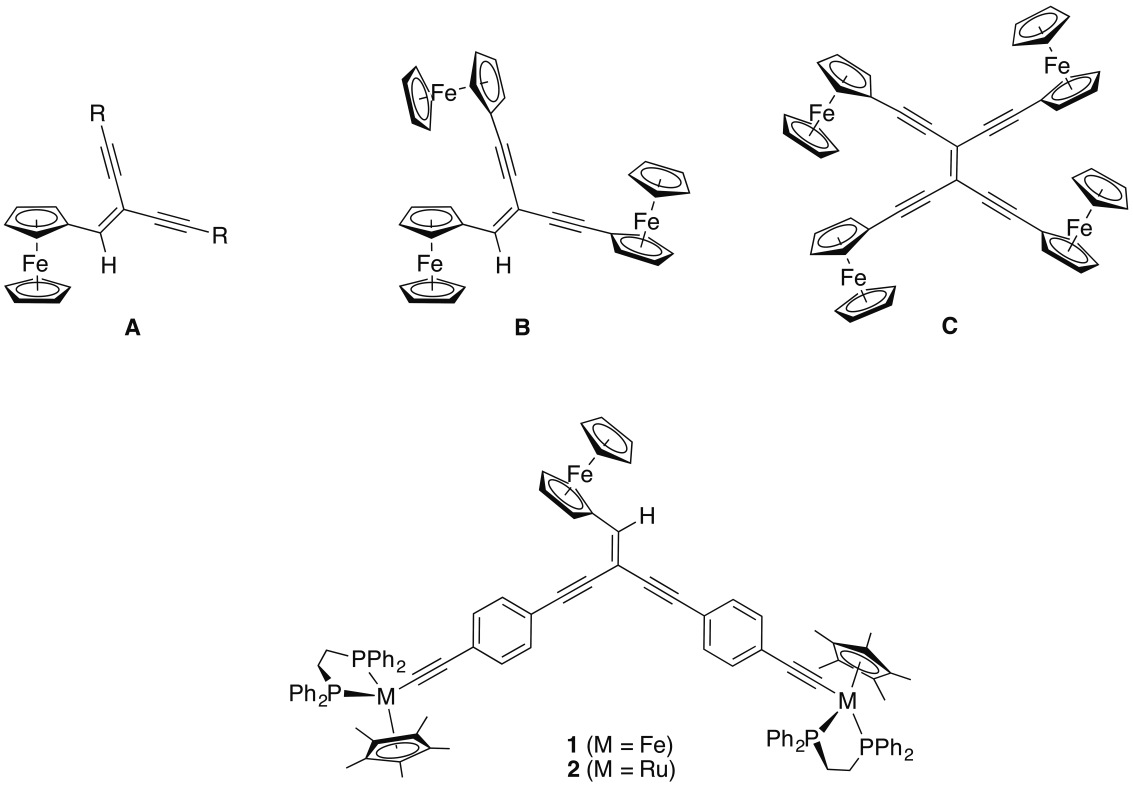

Chart 1

Here we now report the development of an extended derivative of the 1,1-bis(alkynyl)-2-ferrocenylethene building block **A**, and the successful preparation of *bis*-M(dppe)Cp* (M= Fe (**1**), Ru(**2**)) complexes (Chart 1). The electronic structures and intramolecular charge transfer processes through the branched carbon-rich ligand framework within redox families generated from these compounds has been explored through a combination of electrochemical, spectroscopic and computational methods, revealing the subtle differences that arise from the use of the iron and ruthenium end-caps.

RESULTS AND DISCUSSION

1. Syntheses and Characterization. Mono- and binuclear alkynylmetal complexes in the M(dppe)Cp* series (M = Fe, Ru) are usually prepared by one of two general routes.[34, 41-43] Most commonly, the readily available MCl(dppe)Cp* precursor[44] is reacted with a terminal alkyne to give the corresponding vinylidene derivative. In turn, deprotonation of the vinylidene gives the alkynyl metal complex.[43, 45-47] Alternatively, MCl(dppe)Cp* (M = Fe, Ru) can be reacted with a trimethylsilyl-protected alkyne in the presence of a fluoride source (such as KF or NBu_4F) to give the metal alkynyl complex via an in situ desilylation-metallation sequence.[48-54]

In previous investigations by a number of the current authors reaction of $FcCH{=}C(C{\equiv}CH)_2$ with $RuCl(PPh_3)_2Cp$ gave the mono-vinylidene complex $FcCH{=}C(C{\equiv}CH)\{CH{=}CRu(PPh_3)_2Cp\}$. However, all efforts to prepare trimetallic $FcCH{=}C\{C{\equiv}CRu(PPh_3)_2Cp\}_2$ from either $FcCH{=}C(C{\equiv}CH)_2$ or the trimethylsilyl-

protected analogue FcCH=C(C≡CSiMe$_3$)$_2$ proved unsuccessful,[32] likely due to excessive steric crowding.

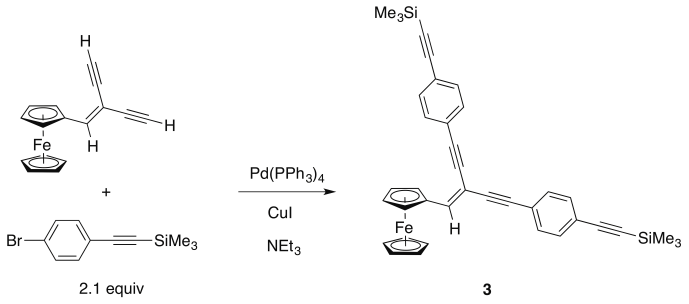

Scheme 1. The synthesis of **3**.

In the current study, Sonogashira cross-coupling of FcCH=C(C≡CH)$_2$[31] with 4-(trimethylsilylethynyl)-bromobenzene was employed to give the 'extended' precursor FcCH=C{1,4-C≡C-C$_6$H$_4$-C≡C-SiMe$_3$}$_2$ (**3**) (Scheme 1). Reaction of **3** with MCl(dppe)Cp* (M = Ru, Fe) and KF in a 1:1 (v/v) mixture of tetrahydrofuran and methanol gave **1** (97%) and **2** (65%) as red and orange powders, respectively (Scheme 2). Potassium *tert*-butoxide was used as both a base and reducing agent during the work-up of the more acidic and oxidatively sensitive homometallic iron complex **1**. Alternatively, **1** could also be obtained via an intermediate bis(vinylidene) complex (Scheme 2). Desilylation of **3** (K_2CO_3 / MeOH) gave FcCH=C{1,4-C≡C-C$_6$H$_4$-C≡C-H}$_2$ (**4**), which was briefly characterised and reacted directly with FeCl(dppe)Cp* in the presence of NH_4PF_6 to give the intermediate vinylidene complex [FcCH=C{1,4-C≡C-C$_6$H$_4$-CH=C=Fe(dppe)Cp*}$_2$](PF$_6$)$_2$ (**5(PF$_6$)$_2$**). Subsequent deprotonation of **5(PF$_6$)$_2$** with KOBu^t gave **1** in quantitative yield.

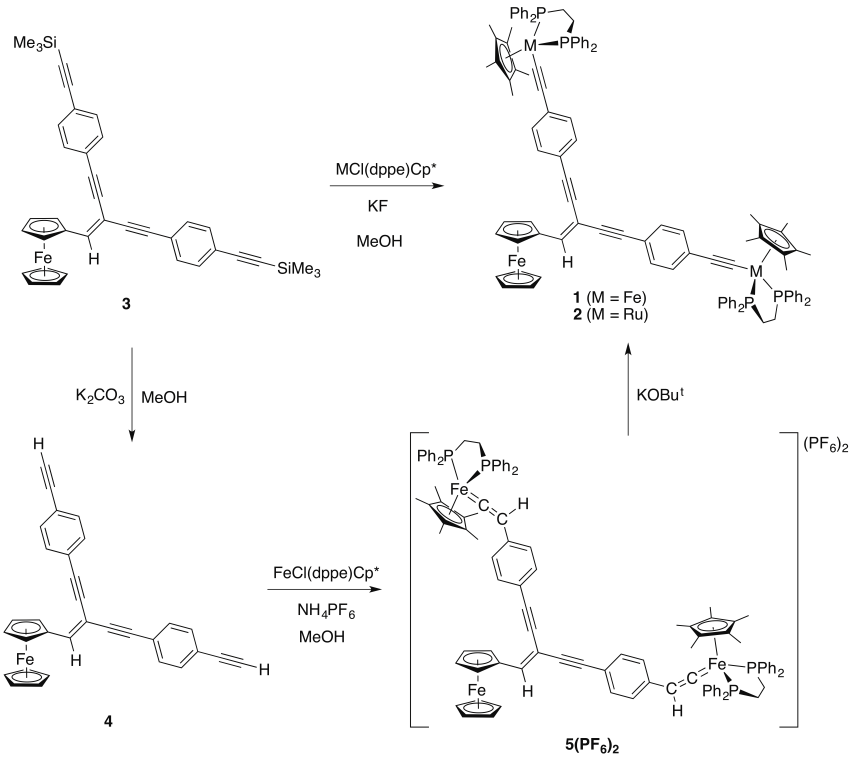

Scheme 2. The synthesis of **1**, **2**, **4** and **5(PF$_6$)$_2$**.

The new complexes **1** and **2** were obtained and characterized by mass spectrometry, IR, ^{1}H and ^{31}P NMR, UV-vis spectroscopies, and cyclic voltammetry. As previously noted for organic derivatives FcCH=C(C≡CR)$_2$,[31] the ^{1}H NMR spectra of **1** and **2** confirm the free rotation of the ferrocenyl moiety around the ferrocene-vinyl C-C bond, with the protons of the η-C_5H_4 ring observed as only two signals (δ_H 4.33, 4.80 (**1**); 4.41, 4.88 (**2**)). In **1**, the vinyl proton resonance is overlapped by the protons of the C_6H_4 ring (δ_H 6.80-6.89), but clearly observed in **2** at δ_H 6.86. The protons of the Cp* ligands attached to the iron atoms in **1** are observed as a single, slightly broadened, resonance (δ_H 1.33 ppm), whilst those in **2** are observed as two very closely spaced, but well-resolved, singlets (δ_H 1.57 and 1.58 ppm) as the *E* and *Z* arms of the double bonds are not strictly

equivalent. However, the electronic and stereochemical differences are not detected in ^{31}P NMR spectra, with the phosphorus atoms on the two M(dppe)Cp* moieties resonating as a singlet at δ_P 99.3 and 80.6 for **1** and **2**, respectively.

The IR spectra of **1** and **2** exhibit strong $\nu_{M\text{-}C\equiv C}$ bands at 2046 and 2062 cm^{-1}, respectively. As generally observed for iron and ruthenium complexes M(C≡CR)(dppe)Cp*, the frequency of the $\nu_{M\text{-}C\equiv C}$ stretch is somewhat higher for the ruthenium complex than for its iron homologue.[55-56] Two weak $\nu_{C\equiv C}$ bands at 2201(sh) and 2187 cm^{-1} (**1**) and a broad stretch at 2189 cm^{-1} (**2**) arise from the triple bonds which connect the vinyl ferrocenyl moiety to the phenyl rings. The spectra of **1** and **2** also show an intense band at 1591/1592 cm^{-1} which can be assigned to the $\nu_{C=C}$ vibration of the vinyl group. The significant intensity of this band is likely due to the dipole across the Cp*(dppe)M-donor ferrocene-acceptor fragment.

2. Cyclic Voltammetry of 1 and 2. The initial scans in the cyclic voltammetry of **1** and **2** were recorded between –1.2 V and 0.6 V (*vs.* $FeCp_2/FeCp_2^+$ at 0.00 V) in 0.1 M NBu_4PF_6 / CH_2Cl_2. In each case, the voltammograms are characterized by two quasi-reversible and well-separated waves, the separation between the anodic and cathodic peaks for each redox wave (ΔE_p = 0.08 ± 0.01 V) being somewhat larger than the value expected for electrochemically reversible systems (ΔE_p = 0.06 V) (Figure 4 and Table 1). The first wave, which consumes approximately double the current of the second, corresponds to the near simultaneous oxidation of the two M(C≡CR)(dppe)Cp* units, while the second waves can safely be assigned to the ferrocenyl moiety. The (i_p^a/i_p^c) current ratios indicate

some chemical irreversibility of the second wave, reflecting chemical instability of the electrochemically-generated trications. In line with these assignments, the first oxidation process(es) of the Fe(dppe)Cp* complex **1** occur some 0.37 V more negative than that of the ruthenium analogue **2**, whilst oxidation potentials assigned to the ferrocenyl groups in **1** and **2** differ by only 0.02 V (Figure 4).

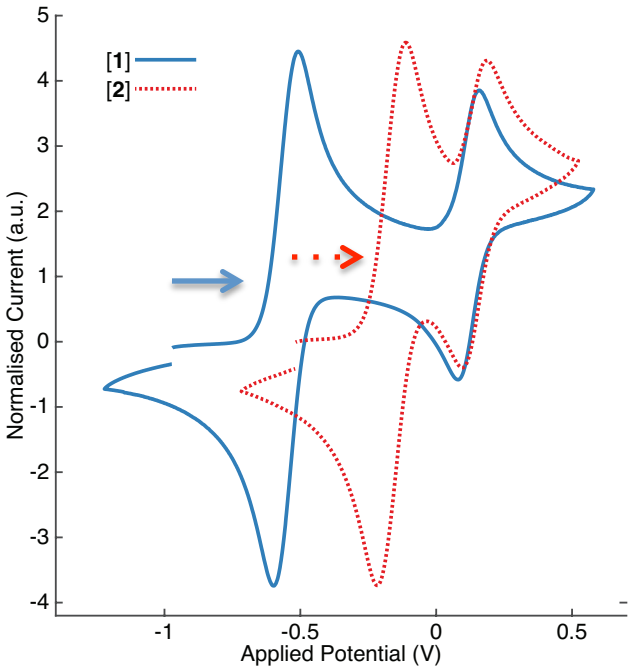

Figure 4. Cyclic voltammograms for **1** (0.2 mM) and **2** (0.2 mM) recorded at $\nu = 0.100$ V s^{-1} in 0.1 M NBu_4PF_6 / CH_2Cl_2.

Table 1. Electrochemical Data[a] for 1 and 2

Cmpd	Redox site	$E_{1/2}$ (V)	ΔEp (V)	i_p^a/i_p^c
1	Fe(dppe)Cp*	-0.55[b]	0.09	0.99
	Fc	+0.12	0.08	0.77
2	Ru(dppe)Cp*	-0.17[b]	0.08	~ 1[c]
	Fc	+0.15	0.09	0.76

[a] Potentials in 0.1 M CH_2Cl_2, $NBu_4(PF_6)$, platinum electrode, sweep rate 0.100 V s^{-1}, potentials are relative to external $FeCp_2/FeCp_2^+$ at 0.00 V (internal reference $Cp_2Co/[Cp_2Co]^+ = -1.30$ V).[57]

[b] Apparent half-wave potential from two unresolved redox processes.

[c] The small separation of the redox processes E(1) and E(2) makes precise measurement of the current ratio i_p^a/i_p^c difficult.

3. In Situ ESR spectra of $1(PF_6)_n$ and $2(PF_6)_n$ (n = 1, 2). The facile oxidation of **1** and **2** revealed by the electrochemical measurements prompted consideration of the redox related products. The complexes **1** and **2** were each reacted with 2 equiv of $[Cp_2Fe](PF_6)$ in THF at -60°C for 1h, and the resulting solutions of $\mathbf{1(PF_6)_2}$ or $\mathbf{2(PF_6)_2}$ transferred in an ESR quartz tube and immediately cooled to liquid nitrogen temperature. ESR monitoring

established that whilst the iron complex diradical is stable in a glass at 66 K (-207 °C) or even as a fluid THF solution below -60 °C, the concentration of ESR active iron species decreases above -40 °C and completely decomposes within 5 minutes at 20 °C.

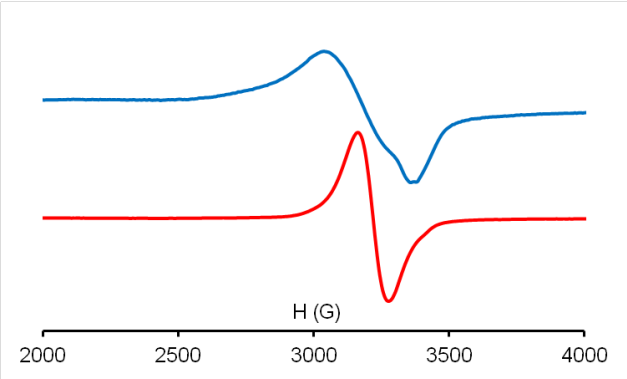

Figure 5. X-band ESR spectrum of **1(PF$_6$)$_2$** (top) and **2(PF$_6$)$_2$** (bottom) at 66 K.

The ESR spectra of **1(PF$_6$)$_2$** and **2(PF$_6$)$_2$** recorded at 66 K (Figure 5) are each characterized by one broad signal (**1(PF$_6$)$_2$**, g = 2.1265; **2(PF$_6$)$_2$**, g = 2.1034) with a width from peak to peak of *ca*. 330 G (**1(PF$_6$)$_2$**) and 120 G for **2(PF$_6$)$_2$** (Figure 5). The ESR spectra of **1(PF$_6$)$_2$** and **2(PF$_6$)$_2$** strongly contrast with the spectra of the iron and ruthenium radical cations [M(C≡CR)(dppe)Cp*]PF$_6$ (M = Fe, Ru) which show one signal with three features (g_1, g_2, and g_3) characteristic of low spin d^5 complexes with a *pseudo*-octahedral geometry,[45, 56, 58] whilst substituted ferrocenyl cations exhibit one signal with two tensor components ($g_{\|}$ and $g_{\perp}$).[59]

In the case of the iron complex **1(PF$_6$)$_2$**, the presence of partially-resolved features in the rather broad ESR spectrum suggests that the signal is close to de-coalescence, consistent with a degree of electron exchange between the Fe(dppe)Cp* and Fc moieties on a rate comparable with the ESR time-scale. In the case of **2(PF$_6$)$_2$**, the ESR spectra shown in

Figure 5 can be regarded as averaged signals resulting from a fast intramolecular electron transfer at the ESR time scale (faster than 10^{-9} s) between the M(dppe)Cp* moieties and the ferrocenyl group. A very similar spectrum was reported by Sato and coworkers for the highly delocalized mixed-valence complex [Cp(dppe)Fe-C≡C-(η-C_5H_4)FeCp](PF_6).[60] Moreover, the smaller value of the *g*-value and the narrower ESR signal obtained for the ruthenium derivatives might result from a larger carbon character of the SOMOs which contains the unpaired electrons.

Given the failure to observe **1(PF$_6$)** in spectroelectrochemical experiments (vide infra), in an additional experiment, complex **1** was reacted with 1 equiv of [Cp_2Fe](PF_6) under the same conditions to give a solution containing **1(PF$_6$)** comproportionated with **1** and **1(PF$_6$)$_2$**. The ESR spectrum collected from this solution is less intense, but otherwise identical that obtained from **2(PF$_6$)$_2$**. In other words, the mono- and di-cations give rise to sufficiently similar ESR spectra that distinction cannot be drawn. This is consistent with DFT calculations in which the spin density in $\mathbf{1}^+$ and $\mathbf{1}^{2+}$ is localized on one or both Fe(dppe)Cp* fragments.

4. IR Spectroelectrochemical Studies of 1(PF$_6$)$_n$ (*n* = 0, 1, 2, 3) and 2(PF$_6$)$_n$ (*n* = 0, 1, 2). UV-vis-NIR and IR spectroelectrochemical investigations were undertaken to complement the electrochemical and ESR studies of the chemically oxidized compounds **1(PF$_6$)$_n$** (n = 0, 1, 2, 3) and **2(PF$_6$)$_n$** (n = 0, 1, 2). In the IR spectra, the stepwise oxidation of **1** and **2** from the neutral species to the dication induces a shift to lower wavenumbers of the $\nu_{M\text{-}C\equiv C}$ bands from 2046 to 1991 cm^{-1} and from 2062 to 1927 cm^{-1} in the iron and

ruthenium series, respectively. As the oxidation of complexes **1** and **2** proceeds, the $\nu_{Fc\text{-}C=C}$ band stretch at 1591/1592 cm^{-1} corresponding to the vinyl group decreases while new less intense band envelopes appear at lower energy, indicating a degree of delocalization along at least one of the M-C≡CCH=CHFc branches.

In the iron series, the intensity of the band corresponding to the neutral complex **1** continuously decreases while the band corresponding to the dication **1(PF$_6$)$_2$** gradually appears. An intermediate band associated with the transient formation of the monocation **1(PF$_6$)** could not be detected. In contrast, for the ruthenium analogue, transient features in the IR spectroelectrochemical experiment were observed at 2131(w), 2040(sh), 1994(m), 1891(s), 1572(m) and 1547(m) cm^{-1} during the oxidation of **2** to **2(PF$_6$)$_2$**, corresponding to the presence of **2(PF$_6$)** in the comproportionated mixture (Figure 6, Table 2). Taken together, the IR spectra suggests that the *E* and *Z* arms of the molecule are completely independent in the iron complexes, while a degree of delocalization leading to enhanced stability of the mixed-valence form **2(PF$_6$)** can be observed in the case of the ruthenium complexes.

On further oxidation of **2(PF$_6$)$_2$** the sample evinced significant and rapid decomposition on the timescale of the spectroelectrochemical experiment, which prevented confident assignment of the resulting spectra. However, in the case of the iron complex oxidation to a trication with sufficient chemical stability to be observed could be achieved, with the assignment being made with confidence following the recovery of the spectrum of the dication on back-reduction. Oxidation of **1(PF$_6$)$_2$** to **1(PF$_6$)$_3$**, which could be followed by

observing the low energy edge of the electronic transitions that fall in the window of the spectrometer (1000 – 10000 cm^{-1}), had little effect on the $\nu_{MC\equiv C}$ and $\nu_{FcC=C}$ IR bands, consistent with a ferrocenyl localised oxidation.

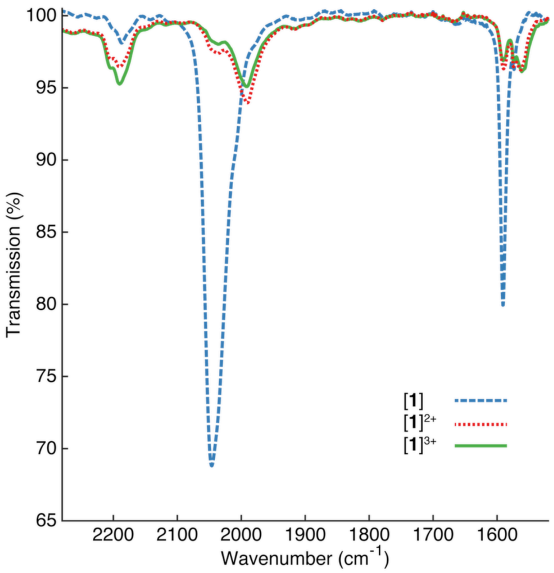
Transmission (%)
Wavenumber (cm-1)
[1]
[1]2+
[1]3+

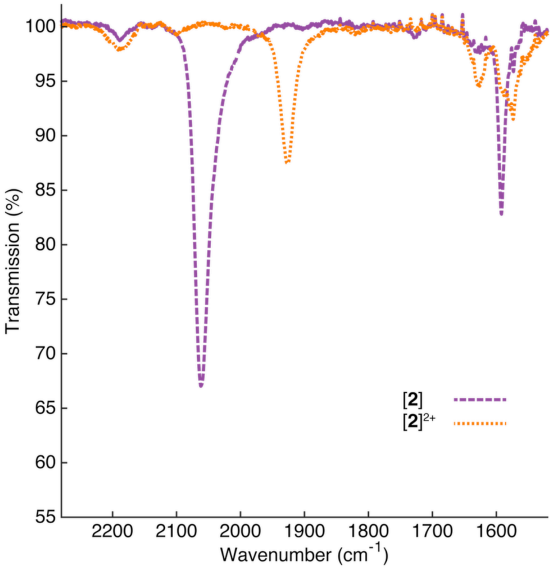
Transmission (%)
Wavenumber (cm-1)
[2]
[2]2+

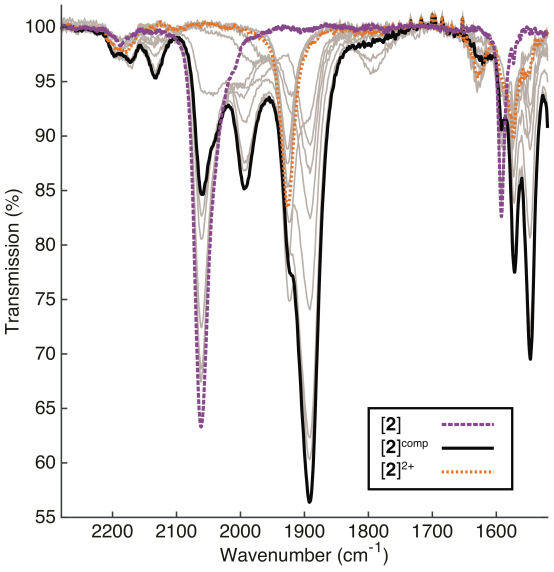
Transmission (%)
Wavenumber (cm-1)
[2]
[2]comp
[2]2+

Figure 6. IR spectra of **1** and **2** collected spectroelectrochemically in 0.1 M CH_2Cl_2/NBu_4PF_6. The spectra of the transiently observed comproportionated mixture between the neutral and dicationic states is shown in solid black trace of the lowest panel, the unique features being attributed to $\mathbf{2}^+$.

Table 2. Characteristic IR data for $\mathbf{1}^{n+}$ and $\mathbf{2}^{n+}$ (n = 0-3) (CH_2Cl_2/0.1 M NBu_4PF_6)

n		**1** (cm^{-1})	*calculated* (km / mol)	**2** (cm^{-1})	*calculated* (km / mol)
0	$\nu_{C\equiv C}$	2202(w,sh), 2187(w)	*2182* (129)	2189(vw)	*2184* (138)
	$\nu_{MC\equiv C}$	2046(vs)	*2047* (1779)	2062(s)	*2057* (2028)
	$\nu_{FcC=C}$	1591(s)	*1590* (278), *1472* (291)	1592(s)	*1590* (314), *1472* (304)
1	$\nu_{C\equiv C}$		*2191* (1148), *2000* (2580)	2135(w)	*2156* (1036)
	$\nu_{MC\equiv C}$		*2040* (1999)	1994(m), 1891(s)	*1953* (62580)
	$\nu_{FcC=C}$ / $\nu_{C=C(Ar)}$		*1548* (2130)	1572(m), 1547(m)	
2	$\nu_{C\equiv C}$	2206(w, sh), 2191(w)	*2181* (436)	2191(w)	*2150* (3974)
	$\nu_{MC\equiv C}$	2045(vw, sh), 1991(w)	*2025* (458)	1927(m)	*1914* (1729)
	$\nu_{FcC=C}$ / $\nu_{C=C(Ar)}$	1590(w), 1574(w), 1563(w)	*1551* (574)	1629(w), 1581(w, br)	*1512* (1975)
3	$\nu_{C\equiv C}$	2205(w, sh), 2190(w)			
	$\nu_{MC\equiv C}$	2040(vw, sh), 1993(w)			
	$\nu_{FcC=C}$ / $\nu_{C=C(Ar)}$	1591(w), 1575(w), 1562(w)			

5. NIR Spectroelectrochemical Studies of $1(PF_6)_n$ (n = 0, 2, 3) and $2(PF_6)_n$ (n = 0, 1, 2). Upon oxidation of **1** to $\mathbf{1(PF_6)_2}$ in the spectroelectrochemical cell (Figure 7, Figure 8), the characteristic MLCT absorption band near 20,000 cm^{-1} [61] collapses giving way to a lower-intensity LMCT feature near 12,000 cm^{-1}.[58] To even lower energy (ca. 5000 cm^{-1}), the characteristic dd (mixed with C≡C π-character) transition of an Fe(III) pseudo-octahedral $[Fe^{III}(C{\equiv}CR)(dppe)Cp^*]^+$ complex can be observed growing in concurrently.[58] Further oxidation to $\mathbf{1(PF_6)_3}$ does not affect the Fe(III) dd transitions associated with the $[Fe^{III}(C{\equiv}CR)(dppe)Cp^*]^+$ moieties, but does cause a collapse of the LMCT band and the appearance of a weak absorption band envelope around 8,000 - 10,000 cm^{-1}. Absorption bands at similar energy have been observed on oxidation of other ferrocenyl ene-diynes, and assigned to the ferrocenium-like dd transitions and LMCT transitions within the vinyl-ferrocenium moiety.[31] These data are consistent with the suggestions made from other spectroscopic observations, with largely independent oxidation of the Fe(dppe)Cp* moieties being followed by oxidation of the ferrocene fragment. There is no detectable absorption band that can be confidently assigned to an intramolecular intervalence charge transfer (or IVCT) transition.

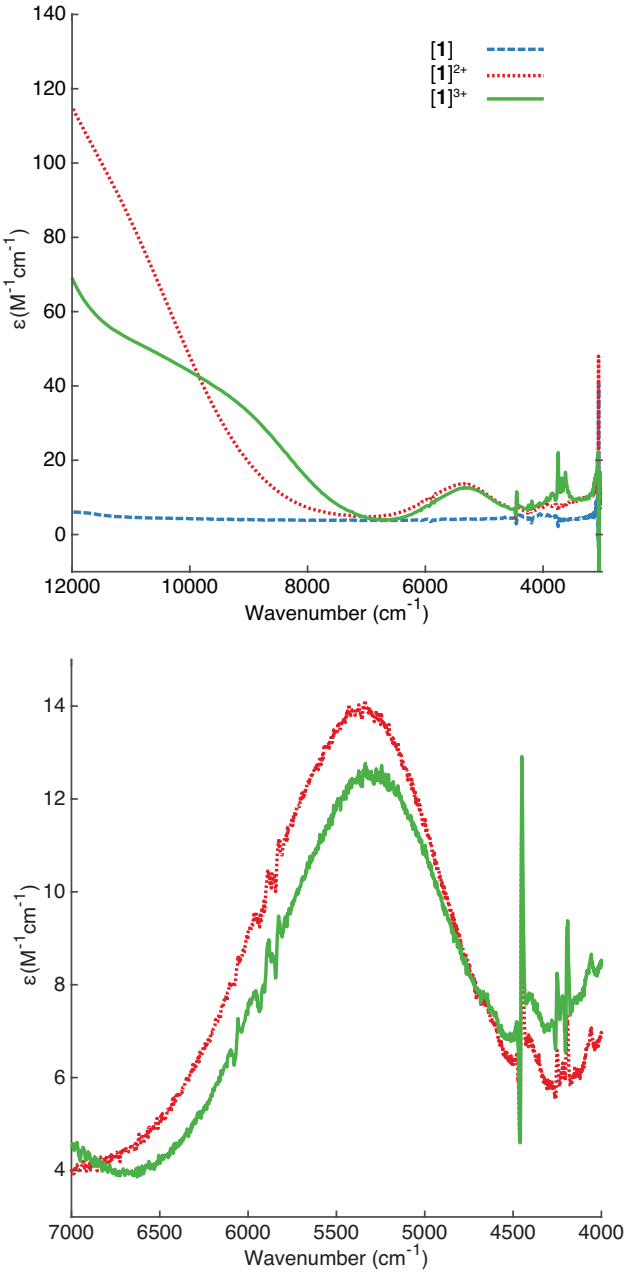

Figure 7. The NIR spectra of $\mathbf{1}^{n+}$ collected spectroelectrochemically (CH_2Cl_2 / 0.1 M NBu_4PF_6) (top). The expansion of the lower energy region (bottom) highlights the extremely weak, approximately Gaussian shaped, bands observed for $\mathbf{1}^{2+}$ and $\mathbf{1}^{3+}$. In this lower energy region, neutral **1** is featureless.

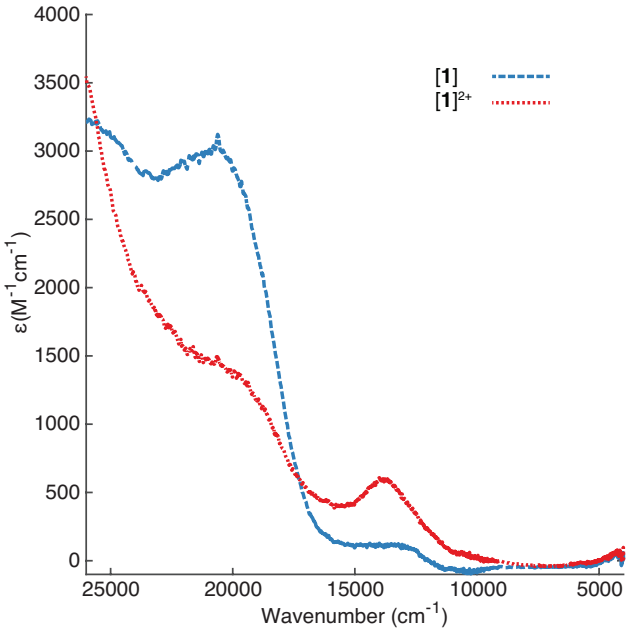

Figure 8. An expanded view of the UV-Vis-NIR spectra of $\mathbf{1}^{n+}$ collected spectroelectrochemically (CH_2Cl_2 / 0.1 M NBu_4PF_6). At this scale the difference between the spectra of $\mathbf{1}^{2+}$ and $\mathbf{1}^{3+}$ cannot be discerned, hence $\mathbf{1}^{3+}$ is omitted.

The step-wise oxidation of the ruthenium-based complex **2** was also carried out in a spectroelectrochemical cell (**Figure 9**). As the potential in the cell is increased to more positive values, the MLCT (or dπ-π*) band near 25,000 cm^{-1}, which typifies Ru(C≡CR)(PP)Cp' complexes,[62] begins to collapse, giving way to a complex series of band envelopes in the NIR region. The band shape evolves with increasing applied potential, with the presence of an isosbestic point near 20,000 cm^{-1} and the reversibility of the spectral changes on the reverse potential sweep consistent with the establishment of the comproportionated equilibrium of **2**, **2(PF$_6$)** and **2(PF$_6$)$_2$**. The definitive assignment of the transitions responsible for the NIR absorption features is an extraordinarily difficult task given the range of conformations that can be adopted by the

rotation of the sandwich, half-sandwich and phenylene moieties relative to each other.[38-40] However, the distinct feature near 5500 cm^{-1} is similar to the IVCT band observed in weakly coupled mixed-valence Ru(dppe)Cp* complexes.[52, 63] This band grows during the early stages of oxidation at lower (less positive) potentials where the equilibrated solution contains **2(PF$_6$)** comproportionated with **2** and **2(PF$_6$)$_2$**, and collapses at higher (more positive) potentials where the solution is expected to be essentially wholly **2(PF$_6$)$_2$**. It is therefore very likely that this band envelope near 5500 cm^{-1} can be assigned to an IVCT transition between the Ru(dppe)Cp* moieties. The NIR bands nearer 10,000 – 15,000 cm^{-1} likely arise from a combination of Fc→$\{C{\equiv}CRu(dppe)Cp^*\}^+$ charge transfer[49, 64-65] and LMCT transitions[62] in **2(PF$_6$)$_2$**, which is the principle species in the solution at higher potentials. Whilst these spectroscopic changes were reversible within the cell, as noted for the IR spectroelectrochemical experiments, attempts to generate **2(PF$_6$)$_3$** by further electrolysis resulted only in extensive decomposition of the sample.

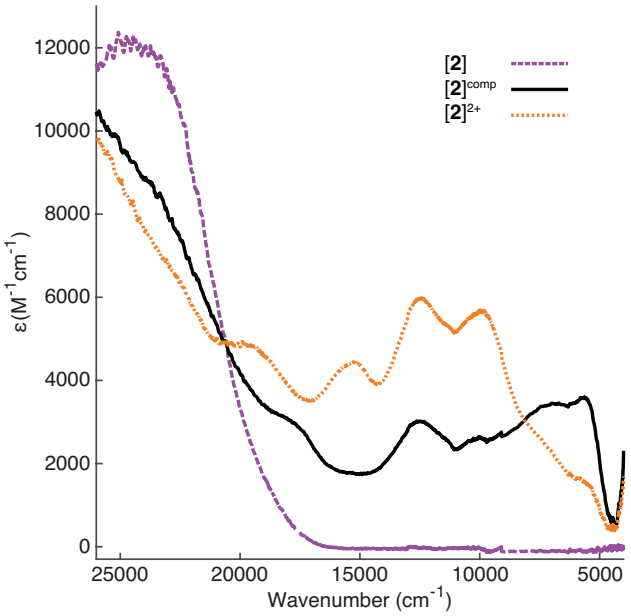

Figure 9. The UV-Vis-NIR spectra of $\mathbf{2}^{n+}$ collected spectroelectrochemically (CH_2Cl_2 / 0.1 M NBu_4PF_6), including the unique spectroscopic features of the comproportionated mixture.

6. Computational studies. Density-functional theory (DFT) calculations were carried out on compounds **1** and **2** and their cationic species to gain further insight into the structural arrangements, electronic structures and bonding properties at the PBE0/LANL2DZ level of theory (see the Experimental Section for computational details), and which complement earlier studies of cross-conjugated carbon scaffolds and complexes cited above and elsewhere.[66-68] The optimized molecular structure of the energetically most stable conformer found in each case and atom labels are shown in Figure 10, and important bond lengths and angles are summarized in Table 3.

Table 3. Important DFT-optimized Bond Lengths (Å) and Angles (°) for Complexes 1^{n+} and 2^{n+} (n = 0-2)

compound	**1**	$\mathbf{1}^{+}$	$\mathbf{1}^{2+\,a}$	**2**	$\mathbf{2}^{+}$	$\mathbf{2}^{2+\,a}$
M2-Cp*[#] (centroid)	1.741	1.742	1.770	1.909	1.918	1.931
M3-Cp*[#] (centroid)	1.741	1.768	1.770	1.908	1.920	1.931
Fe1-Cp[#] (centroid)	1.646/ 1.645	1.647/ 1.646	1.649/ 1.644	1.646/ 1.645	1.654/ 1.649	1.652/ 1.646
M2-C3	1.869	1.846	1.868	1.986	1.952	1.923
M3-C9	1.870	1.855	1.867	1.987	1.944	1.924
C1-C2	1.396	1.373	1.373	1.369	1.384	1.379
C2-C8	1.427	1.424	1.425	1.427	1.417	1.421
C2-C14	1.428	1.425	1.427	1.428	1.418	1.422
C7-C8	1.222	1.222	1.221	1.222	1.225	1.223
C13-C14	1.221	1.222	1.221	1.221	1.225	1.224
C6-C7	1.424	1.423	1.423	1.424	1.415	1.417
C12-C13	1.424	1.418	1.422	1.424	1.412	1.416
C4-C5	1.424	1.421	1.426	1.424	1.410	1.410
C3-C4	1.239	1.240	1.237	1.237	1.246	1.252
C9-C10	1.239	1.238	1.237	1.237	1.248	1.253
M2-P1	2.212	2.212	2.306	2.293	2.309	2.343

M2-P2	2.203	2.204	2.280	2.285	2.300	2.329
M3-P3	2.211	2.295	2.308	2.293	2.313	2.343
M3-P4	2.202	2.274	2.280	2.285	2.304	2.329
M2-C3-C4	176.4	176.1	175.2	175.2	174.5	174.5
M3-C9-C10	176.3	175.7	175.7	175.3	174.6	174.5
C3-C4-C5	179.0	179.6	179.4	179.3	179.4	179.0
C9-C10-C11	179.3	178.7	177.9	179.2	179.1	179.0
C6-C7-C8	179.5	178.4	176.6	179.0	179.0	177.4
C12-C13-C14	179.8	179.5	178.2	179.9	179.7	178.7
C2-C14-C13	179.1	179.3	178.0	179.4	179.9	178.2
C1-C2-C8	124.5	125.0	123.5	124.3	124.1	123.6
C1-C2-C14	119.7	118.7	118.8	119.6	118.6	118.7
τ^{b}	67.6	84.6	114.3	46.0	99.0	156.9

[a] Triplet state configuration. [b] See text.

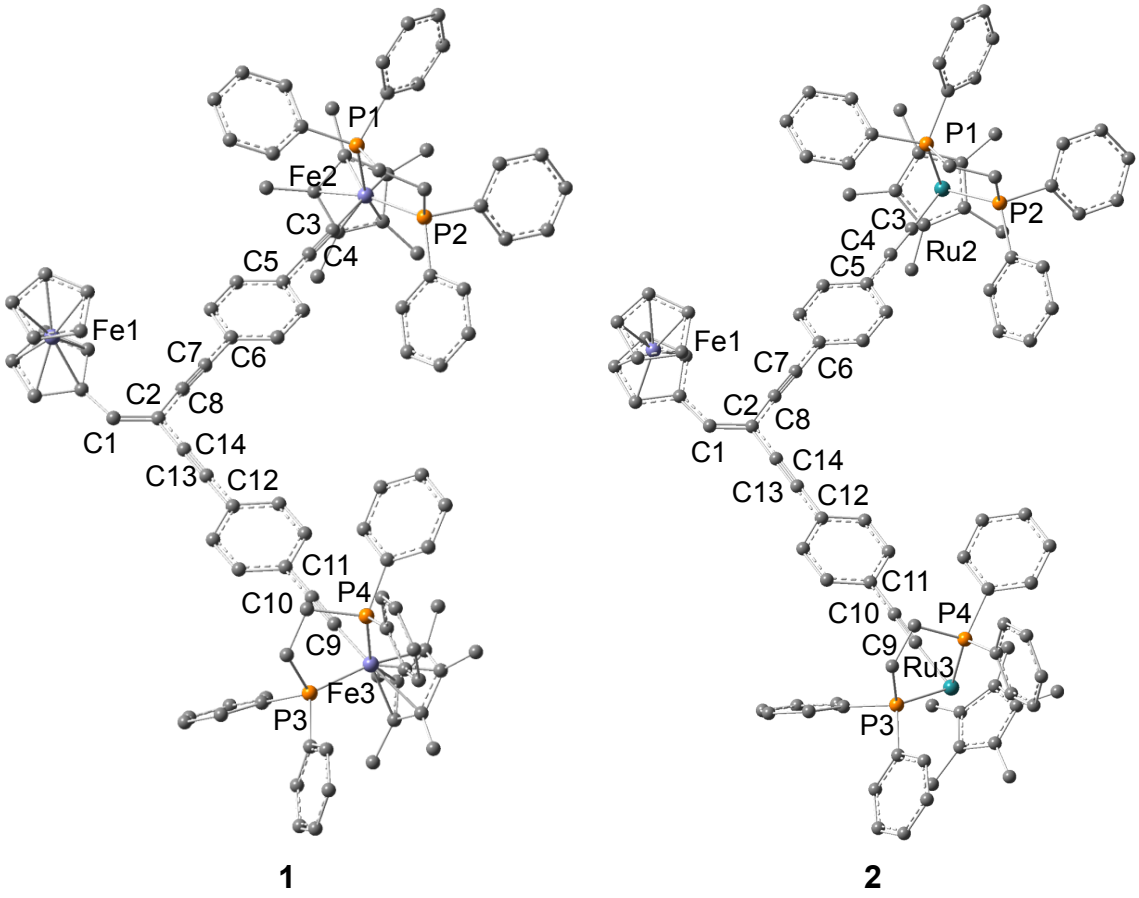

Figure 10. Plots illustrating the DFT-optimized molecular structures of complexes **1** (top) and **2** (bottom). Blue, orange and grey spheres are metal, phosphorus and carbon atoms, respectively. Hydrogen atoms are omitted for clarity.

The molecular geometry around the -C≡C-M(dppe)Cp* end-cap units in **1** (M = Fe) and **2** (M = Ru) is similar to that of model component monometallic complexes Fe(C≡CPh)(dppe)Cp* and Ru(C≡CPh)(dppe)Cp*,[53, 55-56] with bond lengths and angles in the previously established ranges.[34, 69] The two end-caps are twisted relative to each other with the torsion angle (τ) between planes defined by $Cp^{\#}$-M2-M3 and M2-M3-$Cp^{\#}$ ($Cp^{\#}$ represents the centroid of the respective Cp* rings here or Cp in the case of the ferrocenyl moiety described below) determined as τ = 67° and 46° for **1** and **2**, respectively. To

favor π-delocalization, the two phenyl rings are nearly coplanar in both compounds. Concerning the ferrocene moiety, an average Fe-Cp$^{\#}$ distance of 1.65 Å is computed for **1** and **2**. This value compares very well with that experimentally measured in $FeCp_2$.[70]

The HOMOs of complexes **1** and **2** are substantially energetically separated from the LUMO by 3.19 and 3.20 eV, respectively (Figure 11). The nodal properties of the HOMOs of **1** (Figure 12) and **2** (Figure 13) are comparable, forming part of the "t_{2g}" set expected for pseudo-octahedral metal centers, and are π in character, heavily weighed on the metal centers and on the carbon backbone with little to no (HOMO-1) or only a weak (HOMO) contribution of the Fc and ethenyl moieties (Figures 11 - 13). It is noteworthy that the closely lying HOMO and HOMO-1 are not equally distributed over the two branches of the molecules, but rather each largely forms the π-system associated with on 'branch' of the cross-conjugated carbon backbone. These orbitals have significant M2−C3 and M3−C9 anti-bonding and C3−C4 and C9−C10 bonding character. The LUMO of **1** and **2** is mostly centered on the ethenyl group and shows a strong π* character. A noticeable participation of the ferrocenyl moiety in the LUMO of **1** and **2** is observed (Figure 11).

The geometries of the redox related monocationic $\mathbf{1}^{+}$, $\mathbf{2}^{+}$ and dicationic $\mathbf{1}^{2+}$ and $\mathbf{2}^{2+}$ species were also calculated, the results of which are summarized in Table 3 (metrical parameters of only the triplet states are given for the dicationic species, being largely energetically preferred over the singlet states by more than 1.8 eV). In the absence of a complete set of spectroscopic data permitting comparison of $\mathbf{1}^{3+}$ and $\mathbf{2}^{3+}$, these tricationic

species were not calculated. Unsurprisingly given the M-C anti-bonding and C≡C bonding character of the HOMOs, oxidation of **1** and **2** leads to some shortening of the M2−C3 and M3-C9 distances, and a slight lengthening of the adjacent C≡C bonds in the case of **2** (Table 3). The ethenyl C1−C2 bond length remains almost constant across each series. The Fe-C(alkynyl) bond length is rather insensitive to changes in the metal oxidation state in Fe(C≡CR)(dppe)Cp* complexes, differences falling within the experimental statistical differences in the examples that have been crystallographically characterized to date.[58, 61] From the data in Table 3 it can be seen that the Fe2-C3 and Fe3-C9 distances contract by only some 0.02 Å on oxidation of **1** to $\mathbf{1}^{+}$, before elongating again in the triplet dication. The changes in formal metal oxidation state are more readily observed through the Fe-Cp*(centroid) and Fe-P distances. Therefore, if we consider the optimized geometries of **1**, $\mathbf{1}^{+}$ and $\mathbf{1}^{2+}$ we see that on oxidation from **1** to $\mathbf{1}^{+}$ the Fe(3)-$Cp^*_{centroid}$ distance increases from 1.741 to 1.768 Å, and the Fe(3)-P(3)/Fe(3)-P(4) distances elongate from 2.211/2.202 to 2.295/2.274 Å, consistent with oxidation of this metal site, whereas Fe(2) parameters are largely unchanged (i.e. localized oxidation at Fe(3)). On oxidation to $\mathbf{1}^{2+}$, the parameters at Fe(3) remain similar to those of in $\mathbf{1}^{+}$, whilst Fe(2) exhibits the expected changes that accompany oxidation. In contrast, the ruthenium analogues, $[Ru(C{\equiv}CR)(dppe)Cp^*]^{n+}$ feature more Ru-C≡C character in the HOMO/SOMO and hence structural changes are more evident in the Ru-C and C≡C distances on oxidation (Table 3).

Despite the fact that the energies of the HOMO and LUMO are rather similar in both **1** and **2** (Figure 11), the computed adiabatic ionization potentials (IPs) differ; values of

10.53 and 11.39 eV for the dications $\mathbf{1}^{2+}$ and $\mathbf{2}^{2+}$ were found, respectively. The higher IP of $\mathbf{2}^{2+}$ in comparison with that of $\mathbf{1}^{2+}$ is consistent with the higher oxidation potential of **2** than **1** (Table 1). We note that a direct correlation of the gas-phase IPs and electrochemical potentials should not be expected given the sensitivity of the electrochemical data to solvation, ion-pairing, and inner sphere re-organisation energies.

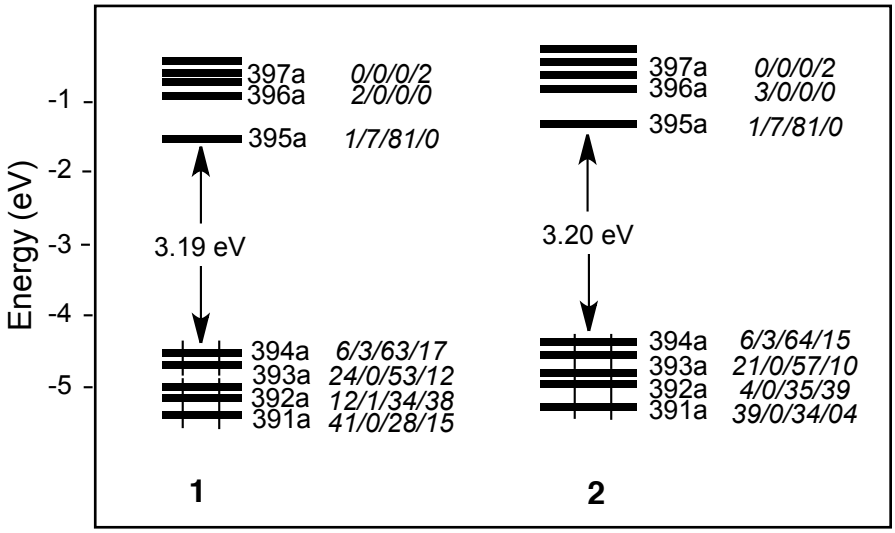

Figure 11. DFT molecular orbital diagram of **1** (left) and **2** (right). M2/Fe1(Fc)/carbon-backbone/M3 percentage contributions are given in italics (M = Fe, Ru).

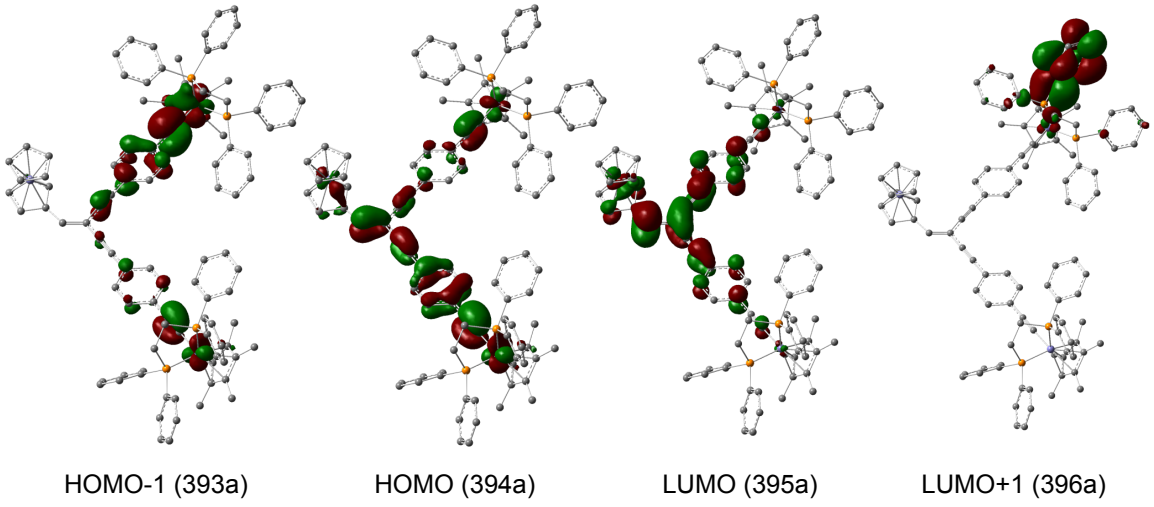

Figure 12. Plots (from left to right) of the HOMO-1 (-4.78 eV), HOMO (-4.63 eV), LUMO (-1.44 eV), and LUMO+1 (-0.85 eV) of complex **1**. Contour values are ± 0.03 $(e/bohr^3)^{1/2}$.

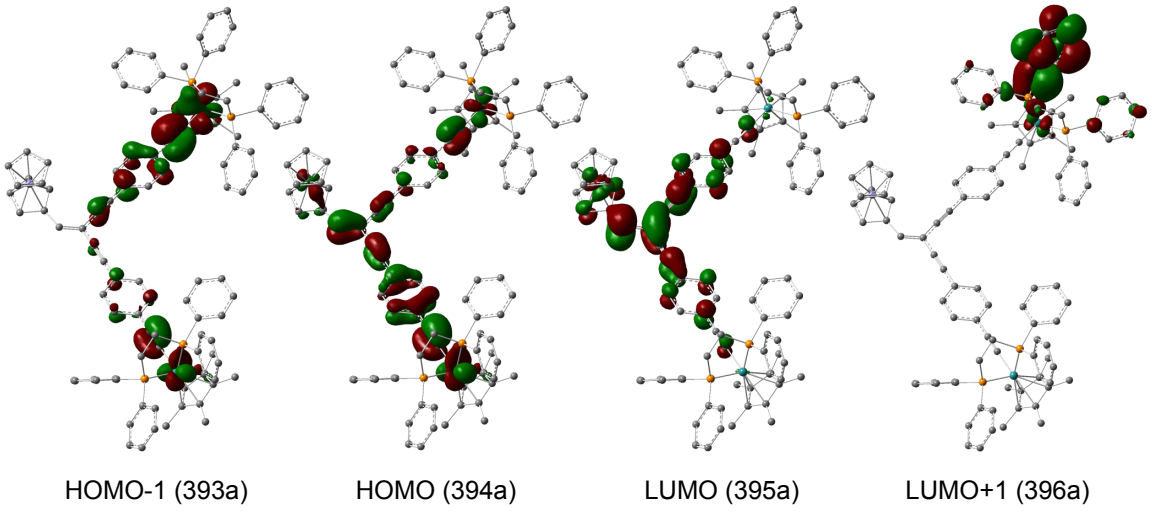

Figure 13. Plots (from left to right) of the HOMO-1 (-4.74 eV), HOMO (-4.59 eV), HOMO-1 (-4.74 eV), LUMO (-1.39 eV), and LUMO+1 (-0.86 eV) of complex **2**. Contour values are ± 0.03 $(e/bohr^3)^{1/2}$.

The energies of the key molecular vibrations were computed for $\mathbf{1}^{n+}$ and $\mathbf{2}^{n+}$ (n = 0-2) to provide a point of reference between the experimental observations and the computational results. For the neutral complexes **1** and **2,** the $\nu_{M\text{-}C\equiv C}$ and $\nu_{C\equiv C}$ vibrational frequencies are computed at 2047 cm^{-1} (1779 km/mol) and 2183 cm^{-1} (129 km/mol) (**1**) and at 2057 cm^{-1} (2028 km/mol) and 2184 cm^{-1} (138 km/mol) (**2**) in excellent agreement with the experimentally determined values (Table 2). The vinyl $\nu_{C=C}$ bands are calculated at 1472 cm^{-1} (291 km/mol) and 1590 cm^{-1} (278 km/mol) for **1**, and 1472 cm^{-1} (304 km/mol) and 1590 cm^{-1} (314 km/mol) for **2**. Again, these values are in excellent agreement with the observed bands at 1591 and 1592 cm^{-1}, the bands calculated to fall below 1500 cm^{-1} not being clearly resolved in the experimental spectra. For the monocationic system $\mathbf{1}^{+}$ for which no experimental values are observed, strong and moderate $\nu_{C\equiv C}$ bands are calculated at 2000 cm^{-1} (2580 km/mol) and 2191 cm^{-1} (1148 km/mol) whereas a $\nu_{M\text{-}C\equiv C}$ band is calculated at 2040 cm^{-1} (1999 km/mol). Overall, these values reflect localized oxidation of one Fe(dppe)Cp* moiety. The vinyl $\nu_{C=C}$ band shifts somewhat to 1548 cm^{-1} (2130 km/mol) for $\mathbf{1}^{+}$.

In the case of $\mathbf{2}^{+}$, a very intense $\nu_{M\text{-}C\equiv C}$ band is calculated at 1953 cm^{-1} (62580 km/mol) and involved a coupled oscillation of both Ru-C≡C fragments. Vibration of the C≡C bonds associated with the vinyl moiety are calculated at 2156 cm^{-1} (1036 km/mol). The very high oscillator strength of the $\nu_{MC\equiv C}$ arising from vibration along the electron-transfer axis in $\mathbf{2}^{+}$ accounts for the observation of a band from this species in the experimental spectroelectrochemical experiment, despite the low equilibrium concentration of this species.

For the dicationic (triplet) system $\mathbf{1}^{2+}$, two moderately intense $\nu_{MC\equiv C}$ and $\nu_{C\equiv C}$ vibrations are calculated at 2025 cm^{-1} (458 km/mol) and 2181 cm^{-1} (436 km/mol), respectively, whilst the vinyl $\nu_{C=C}$ at 1551 cm^{-1} (574 km/mol) would be experimentally indistiguishable from that in $\mathbf{1}^{+}$. These values compare very well with the spectroelectrochemically observed bands at 2191 ($\nu_{C\equiv C}$), 1991 ($\nu_{MC\equiv C}$) and 1563 ($\nu_{C=C}$) cm^{-1}. The observation of additional bands in the experimental spectra is not unexpected given the conformational flexibility of these complexes with regards to the dihedral angles between the key Fe(dppe)Cp*, C_6H_4 and Fc moieties. For the Ru analogue $\mathbf{2}^{2+}$, $\nu_{MC\equiv C}$ and $\nu_{C\equiv C}$ vibrations are calculated at 1914 cm^{-1} (1729 km/mol) and 2150 cm^{-1} (3974 km/mol), respectively. The vinyl $\nu_{C=C}$ vibration is computed at 1512 cm^{-1} (1975 km/mol). These values are comparable to those experimentally measured (Table 2).

With the vibrational data giving confidence in the relevance of the optimized molecular geometries to the experimental samples, attention was turned to further exploration of the electronic structures. Mulliken atomic spin densities of the monocationic species $\mathbf{1}^{+}$ and $\mathbf{2}^{+}$ species were computed and compared to gain insight concerning the (de)localization of the unpaired electron over the molecule, as well as some indication about the electronic communication between the metal end-groups *via* the Fc-carbon backbone. Results reveal a quite asymmetric iron cation $\mathbf{1}^{+}$ with the unpaired electron mostly localized on one branch, especially on the -C≡C-Fe(dppe)Cp* end-cap unit (Figure 14, left). The spin density on Fc is very small (0.02 e), indicating that the oxidation occurs mainly at one iron-ethynyl unit. For $\mathbf{2}^{+}$, the situation differs with the unpaired electron more

extensively delocalized over the whole molecule with comparable contribution on the Ru atoms and Fc (Ru2: 0.13 e, Ru3: 0.17 e, Fc: 0.12 e, carbon backbone: 0.88 e) (Figure 14, right). This indicates that electron density is removed from three metal centers and the carbon backbone upon oxidation of **2**. Finally, it is worth mentioning that a more substantial spin density on the β-carbon atom close to the ferrocenyl group, is computed for $\mathbf{2}^{+}$ (0.20 e) than $\mathbf{1}^{+}$ (0.04 e).

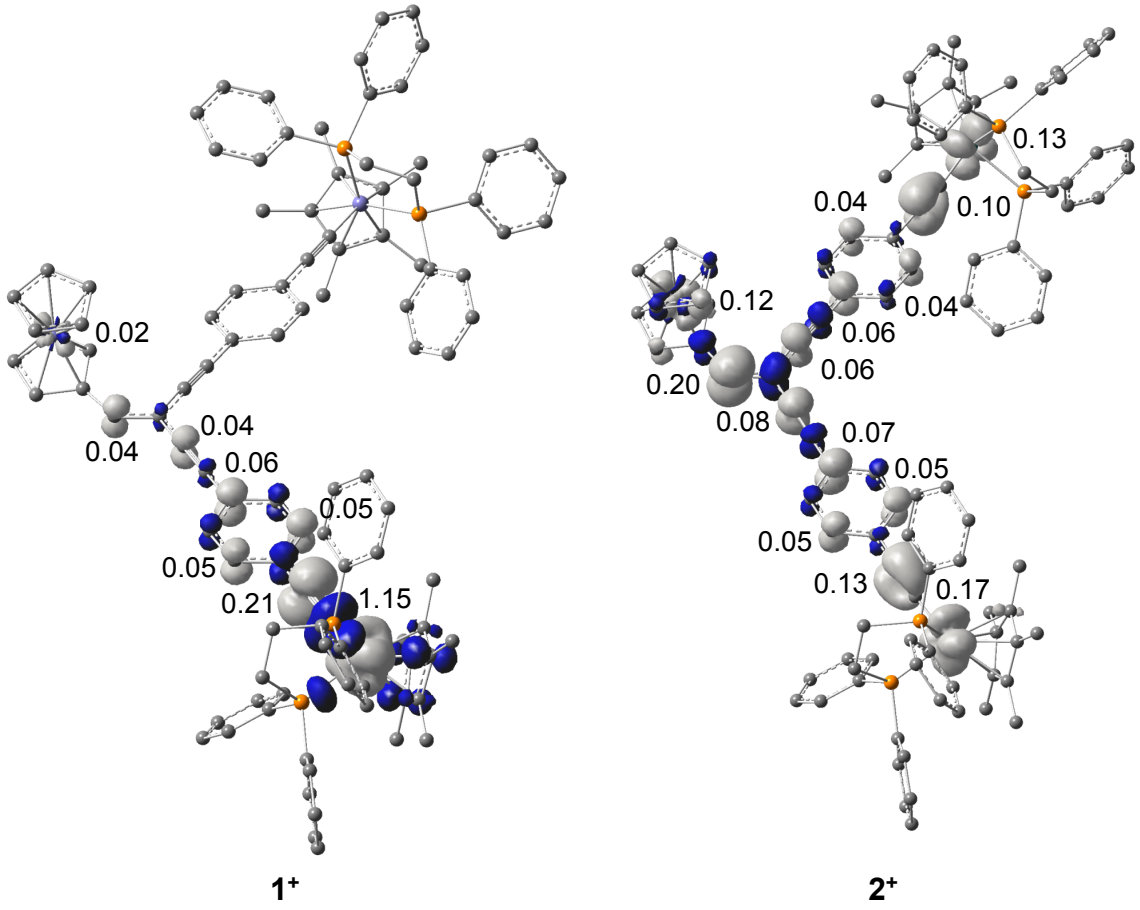

Figure 14. Spatial distribution of the computed spin density of $\mathbf{1}^{+}$ (left) and $\mathbf{2}^{+}$ (right). Isocontour value: ± 0.002 e/bohr^3.

Mulliken atomic spin densities of the dicationic species $\mathbf{1}^{2+}$ and $\mathbf{2}^{2+}$ with their triplet electronic configuration were also computed (Figure 15). Note that the broken-symmetry singlet (BS) featuring the antiferromagnetic states, are computed to be almost isoenergetic (less stable by 0.001 eV (ca. 0.2 kcal/mol)). For the iron species, the spin density is mainly localized on the iron atoms of the Fe(dppe)Cp* fragments (Fe2: 1.13 e and Fe3: 1.13 e) and to a lesser extent on the carbon bridge (0.67 e), consistent with the formal assignment of Fe(III) oxidation states for these fragments. The contribution on the Fe atom of the ferrocenyl (Fc) moiety is very weak (0.02 e). In the case of the ruthenium species, the spin density is more evenly distributed over the whole molecule with 1.69 e on the carbon bridge and 0.47 and 0.46 e on the Ru2 and Ru3 ruthenium centers, respectively. Note that whilst the participation of the ferrocenyl iron atom Fe1 is small (0.07 e), this is still significantly greater than in the iron species (0.02 e).

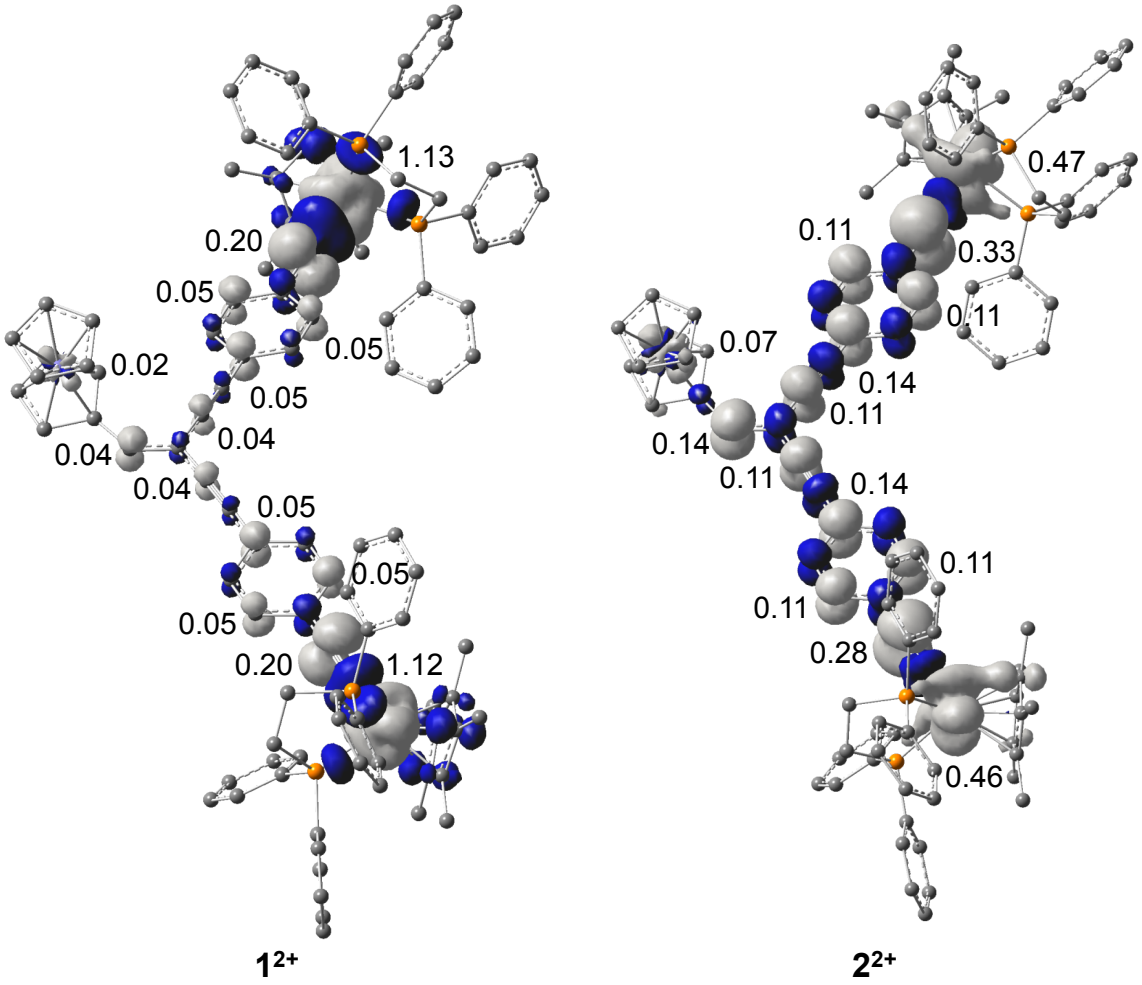

Figure 15. Spatial distribution of the computed spin density of the triplet state of $\mathbf{1}^{2+}$ (left) and $\mathbf{2}^{2+}$ (right). Isocontour value: ± 0.002 e/bohr^3.

ESR properties of the complexes $\mathbf{1}^{n+}$ (n = 1, 2) and $\mathbf{2}^{n+}$ (n = 1, 2) were also computed. The resulting g-tensor components are given in Table 4 for a comparison with experiment. The agreement is moderately satisfactory although the computed values indicate some anisotropy of the rhombic g-tensor ($\Delta g = g_1 - g_3$) for both compounds, which is not observed experimentally. Moreover, the values calculated for $\mathbf{1}^{+}$ and $\mathbf{1}^{2+}$ differ substantially; this suggests that the concentration of $\mathbf{1}^{+}$ in the comproportionated

mixture studied experimentally is too low to be observed. In addition, the small values of Δg computed for the mono-oxidized forms $\mathbf{1}^+$ (0.111) and $\mathbf{2}^+$ (0.069) are consistent with an important degree of delocalization of the odd electron in these mixed-valence species, especially for the ruthenium compound.[34] However, these results must me taken with caution, as it is known that the rotational orientation of the M(dppe)Cp* fragments around the M-C≡C axis relative to the conjugated ligand can strongly influence the *g*-tensor values.[71] Despite these ambiguities, the smaller values of the *g*-tensor components for $\mathbf{2}^+$ and $\mathbf{2}^{2+}$ with respect to $\mathbf{1}^+$ and $\mathbf{1}^{2+}$ reflects more delocalization in the ruthenium compounds as inferred from the experimental spectroscopic data and electronic structure calculations.

In order to explore the involvement of the Fc group in the ESR properties of $\mathbf{1}^{n+}$ and $\mathbf{2}^{n+}$ (n = 1, 2), *g*-tensor computations were performed on the iron models $[FcCH=CH_2]^+$ ($\mathbf{6}^+$) and $[CH_2=C\{1,4\text{-}C\equiv C\text{-}C_6H_4\text{-}C\equiv C\text{-}Fe(dppe)Cp^*\}_2]^+$ ($\mathbf{7}^+$) for comparison. As expected, an axial *g*-tensor is obtained for $\mathbf{6}^+$ with two different tensor components ($g_{\parallel}$ = 1.173) and $g_{\perp}$ = 4.473). Such values are comparable to those expected for Fc^+ complexes.[72-74] Computations on model $\mathbf{7}^+$ predict a g_{iso} value of 2.079 and a rhombic splitting of the *g*-tensor with g_1 = 1.994, g_2 = 2.105, and g_3 = 2.140 which very slightly differs from that computed for $\mathbf{1}^+$ (Table 4). These results seem to indicate a relatively minor role of the Fc group on the ESR properties of $\mathbf{1}^{n+}$ and $\mathbf{2}^{n+}$.

Table 4. Computed (*Experimental*) ESR Parameters for $\mathbf{1}^{n+}$ and $\mathbf{2}^{n+}$ (n= 1, 2)

compound	g_1	g_2	g_3	g_{iso}	Δg
$\mathbf{1}^{+}$	2.003	2.083	2.114	2.067 (*2.1265*)	0.111
$\mathbf{1}^{2+}$	1.980	2.114	2.222	2.106 (*2.1265*)	0.242
$\mathbf{2}^{+}$	2.006	2.044	2 .075	2.042	0.069
$\mathbf{2}^{2+}$	1.880	1.947	2.019	1.949 (*2.1034*)	0.139
$\mathbf{6}^{+}$	1.165	1.181	4.473	2.273	3.308
$\mathbf{7}^{+}$	1.994	2.105	2.140	2.079	0.146

CONCLUSION

The complexes FcCH=C{1,4-C≡C-C_6H_4-C≡CM(dppe)Cp*}$_2$ (Fc = ferrocenyl (FeCp(η-C_5H_4-); M = Fe (**1**), Ru (**2**)) and their redox-related products have provided further opportunities to explore the electronic differences and characteristics of putative mixed-valence complexes derived from the half-sandwich {M(dppe)Cp*} moieties, and through an 'extended' cross-conjugated bridging ligand. Despite the low (unresolved) separation of the first two oxidation processes, in the case of the ruthenium species **2** a combination of UV-vis-NIR and IR spectroelectrochemistry can be used to detected the presence of mixed-valence $\mathbf{2}^{+}$ in the comproportioned mixture. Electron exchange between the metal-

complex 'branches' of $\mathbf{2}^+$ appears to be fast on the EPR, with the significant contributions from the carbon chain and organic-like singlet in the EPR spectrum. Quantum chemical analysis supports the description of $\mathbf{2}^+$ in terms of a polarized, but still rather extensively delocalised, system with substantial spin-density over the bridging ligand framework. In contrast, the iron complex **1** gives rise too much more metal-localized redox-behavior. Apparently the more limited delocalization into the carbon-rich bridging ligand lowers the thermodynamic stability of mixed-valence $\mathbf{1}^+$, which cannot be detected spectroscopically using the methods available here. Thus, as has been observed recently in linearly conjugated systems,[37] the limited d-π mixing associated with 3d metals such as Fe promotes more localized behavior in mixed-valence complexes featuring carbon-rich bridging ligands, whilst heavier 4d metals such as Ru mix more extensively with the ligand leading to more bridge-based redox character.

EXPERIMENTAL SECTION

All reactions were carried out using standard Schlenk techniques under dry, inert atmospheres of argon (reactions involving FeCl(dppe)Cp*) or nitrogen (all other reactions). Triethylamine was distilled over potassium hydroxide, hexanes, diethyl ether and tetrahydrofuran were dried by passage over an alumina column or distilled from sodium benzophenone ketyl. Methanol was dried and distilled from magnesium methoxide. Dichloromethane was dried either by distillation under argon from P_2O_5 and then Na_2CO_3 or on an Inert Technologies solvent purification system. Triethylamine and methanol were further deoxygenated by sparging with N_2 or Ar before use. Other solvents were standard reagent grade and used as received. No special precautions were taken to

exclude air or moisture during workup except where otherwise indicated. The compounds $FeCl(dppe)Cp^*{\bullet}CH_2Cl_2$ and $RuCl(dppe)Cp^*$,[44] $FcCH{=}C\{C{\equiv}CH\}_2$[31] and $Pd(PPh_3)_4$[75] were prepared according to published procedures. The compound 4-(trimethylsilylethynyl)bromo benzene was prepared by a minor variation of the published route,[76] as detailed in the SI. Other chemicals were purchased from commercial sources and used without further purification.

Instruments. Solid-state infrared spectra were obtained as KBr Pellets with a Bruker IFS28 FT-IR infrared spectrophotometer (4000-400 cm^{-1}) and solution spectra on a Cary 660 . Near-IR and UV-visible spectra were recorded in solution using a 1cm long quartz cell on a Cary 5000 spectrophotometer. NMR spectra were recorded at 25 °C on a Bruker Avance III 600 (^1H, 600.1 MHz; ^{13}C, 150.9 MHz; ^{31}P, 242.9 MHz), A Bruker Avance III 500 (^1H, 500.1 MHz; ^{13}C, 125.8 MHz; ^{31}P, 202.4 MHz) or a Bruker Avance 400 (^1H, 400.1 MHz; ^{13}C, 100.6 MHz) spectrometer using $CDCl_3$ or CD_2Cl_2 as the solvent. Chemical shifts (ppm) were determined relative to internal residual solvent signals (^1H, ^{13}C)[77] or external 85% H_3PO_4 (^{31}P δ = 0.0 ppm). Cyclic voltammetry was carried out in a nitrogen filled glove box using a PalmSens Emstat^{3+} potentiostat, with platinum working electrode, a platinum plated titanium wire counter electrode, and a platinum plated titanium wire pseudo-reference electrode, from solutions of the complex (ca. 0.2 mM) in dichloromethane containing 0.1 M NBu_4PF_6 as the electrolyte, ν = 100 mVs^{-1}. The cobaltocene/cobaltocinium couple was used as an internal reference for potential measurements such that $Cp_2Co/[Cp_2Co]^+$ falls at –1.30 V relative to external $Cp_2Fe/[Cp_2Fe]^+$ at 0.00 V.[40] Electron spin resonance (ESR) spectra were recorded on a

Bruker EMX-8/2.7 (X-band) spectrometer at 77K (liquid nitrogen). Spectroelectrochemistry was conducted in an OTTLE cell,[78] using solutions in dichloromethane containing 0.1 M nBu$_4$NPF$_6$ as the supporting electrolyte. Spectra were recorded on an Agilent Technologies Cary 660 FT-IR, an Agilent Technologies Cary 5000 UV–Vis–NIR or an Avantes diode array UV-Vis-NIR system comprising two light sources (UV-Vis: AvaLight-DH-S-Bal, Vis-NIR: AvaLight-Hal-S) and two spectrometers (UV-Vis: AvaSpec-ULS204-8L-USB2, NIR: AvaSpec-NIR256-2.5TEC) connected to a custom-built sample holder by bifurcated fibre optic cables. The Vis-NIR light source was attenuated with a band-pass filter transparent between ~900–4700 nm. Mass spectrometry was carried out employing ASAP (APCI), ESI, MALDI or EI ionization techniques. Elemental analyses were performed at the London Metropolitan University.

FcCH=C{1,4-C≡C-C$_6$H$_4$-C≡CSiMe$_3$}$_2$ (**3**) A mixture of FcCH=C{C≡CH}$_2$ (762 mg, 2.93 mmol), 4-(trimethylsilylethynyl)bromo benzene (1.56g, 6.15 mmol), Pd(PPh$_3$)$_4$ (160mg, 147 μmol), CuI (28.0 mg, 147 μmol) and triethylamine (50 mL) was heated at reflux for 17 h and then allowed to cool to ambient temperature. Following removal of the solvent, the residue was purified by column chromatography (eluent: hexanes/ethyl acetate (98:2 (v/v))) to afford FcCH=C{1,4-C≡C-C$_6$H$_4$-C≡CSiMe$_3$}$_2$ as a red solid (661 mg, ~80% purity by ^{1}H NMR). Analytically pure FcCH=C{1,4-C≡C-C$_6$H$_4$-C≡CSiMe$_3$}$_2$ was obtained following preparative TLC of this solid (eluent: hexanes/ethyl acetate (98:2 (v/v))) which was carried out in small batches immediately prior to its use in further reactions. For a typical preparative TLC purification, 109 mg of crude **3** gave 53 mg of pure product. ^{1}H NMR (500 MHz, CDCl$_3$): δ = 0.26 (s, 9H, Si(CH_3)$_3$), 0.27 (s,

9H, Si(CH_3)$_3$), 4.22 (5H, s, C$_5H_5$), 4.55 (m, 2H, C$_5H_4$), 4.88 (m, 2H, C$_5H_4$), 6.99 (s, 1H, C=C*H*), 7.41 – 7.51 (m, 8H, C$_6H_4$). ^{13}C NMR (125 MHz, $CDCl_3$): δ = 0.07 (Si(*C*H$_3$)$_3$), 69.9 (*C*$_5$H$_5$), 70.0 (*C*–H, C$_5$H$_4$), 70.9 (*C*–H, C$_5$H$_4$), 79.6 (*C*–CH=C, C$_5$H$_4$), 87.3 (*C*≡C), 89.8 (*C*≡C), 91.6 (*C*=C–H), 93.3 (*C*≡C), 96.4 (C≡*C*–Si), 96.7 (C≡*C*–Si), 98.9 (*C*≡C), 104.8 (*C*≡C), 104.9 (*C*≡C), 122.8 (*C*–C≡C, C$_6$H$_4$), 123.2 (*C*–C≡C, C$_6$H$_4$), 123.5 (*C*–C≡C, C$_6$H$_4$), 123.5 (*C*–C≡C, C$_6$H$_4$), 131.3 (*C*–H, C$_6$H$_4$), 131.4 (*C*–H, C$_6$H$_4$), 132.0 (*C*–H, C$_6$H$_4$), 132.2 (*C*–H, C$_6$H$_4$), 145.6 (C=*C*–H). FT-IR (CH_2Cl_2) ν 2209 (C≡C), 2156 (C≡C–Si), 1576 cm^{-1} (C=C). ASAP-MS(+): *m/z* 605.2 [M + H]$^+$. Anal. Calcd For $C_{38}H_{36}Si_2Fe$: C, 75.48; H, 6.00. Found: C, 75.40; H, 6.12.

FcCH=C{1,4-C≡C-C$_6$H$_4$-C≡CH}$_2$ (4). A Schlenk tube was charged with FcCH=C{1,4-C≡C-C$_6$H$_4$-C≡CSiMe$_3$}$_2$ (218 mg, 0.36 mmol), an excess of K_2CO_3 (299 mg, 2.76 mmol, 6 equiv) and the solids dissolved in 2:1 MeOH:THF (18 mL). The reaction was stirred at room temperature for 4 h, after which the solvents were removed under reduced pressure and the solid residue extracted with diethyl ether. The extracts were combined, the solvent was removed under reduced pressure, and the resulting red powder dried *in vacuo* for 1 h to yield **4**, which was briefly characterized before further use (166 mg, 0.36 mmol, nominally 100%) . ^{1}H NMR (400 MHz, $CDCl_3$): δ = 2.98 (s, 1H, C≡C*H*), 3.00 (s, 1H, C≡C*H*), 4.02 (s, 5H, C$_5H_5$), 4.25 (s, 2H, C$_5H_4$), 4.69 (s, 2H, C$_5H_4$), 6.82 (s, 1H, C=C*H*), 7.06 (s, 2H, C$_6$H$_4$), 7.26 (s, 2H, C$_6$H$_4$), 7.31 (m, 4H, C$_6$H$_4$).

[FcCH=C{1,4-C≡C-C$_6$H$_4$-CH=C=Fe(dppe)Cp*}$_2$](PF$_6$)$_2$ (5(PF$_6$)$_2$). A Schlenk tube was charged with a freshly prepared sample of **4** (149 mg, 0.32 mmol)

FeCl(dppe)Cp*•CH_2Cl_2 (477 mg, 0.67 mmol, 2.1 equiv), and NH_4PF_6 (109 mg, 0.67 mmol), before addition of 2:1 MeOH:THF (15 mL). The reaction medium was stirred at r.t. for 48 h, the solvents removed and the product extracted with dichloromethane (2 x 10 mL). The combined extracts were concentrated to 5 mL under vacuum, and addition of methanol (15 mL) caused the precipitation of a red solid that was collected by filtration, washed with methanol (3 x 10 mL) and dried in vacuo to afford **5(PF$_6$)$_2$** (401 mg, 0.208 mmol, 65%), as a red powder. ^{1}H NMR (400 MHz, $CDCl_3$): δ = 1.51 (s, 30H, $C_5(CH_3)_5$), 2.42 (m, 4H, CH_2), 2.98 (m, 4H, CH_2), 4.15 (s, 5H, C_5H_5), 4.40 (s, 2H, C_5H_4), 4.81 (s, 2H, C_5H_4), 5.04 (m, 2H, Fe=C=C*H*), 6.21 (m, 2H, C_6H_4), 6.51 (m, 2 H, C_6H_4), 6.90 (s, 1 H, C=C*H*), 7.02 (m, 2 H, C_6H_4), 7.10 (m, 10H, C_6H_4+*m*-C_6H_5/$_{dppe}$), 7.26 (m, 8H, *m*-C_6H_5/$_{dppe}$), 7.39 (m, 16H, *o*-C_6H_5/$_{dppe}$), 7.52 (m, 8H, *p*-C_6H_5/$_{dppe}$). ^{31}P NMR (162 MHz, $CDCl_3$): δ = 86.5 (s, dppe), 86.6 (s, dppe), -144.5 (septet, $^1J_{P\text{-}F}$ = 710 Hz, PF_6). FT-IR (KBr) *v* 2184 s (C≡C), 1640 s (Fe=C=C), 831 s (PF_6) cm^{-1}.

FcCH=C{1,4-C≡C-C$_6$H$_4$-C≡C-Fe(dppe)Cp*}$_2$ (1). Route A: Potassium fluoride (8.0 mg, 130 μmol) and FeCl(dppe)Cp*•CH_2Cl_2 (98 mg, 138 μmol) were added to a solution of **3** (42 mg, 69 μmol) in tetrahydrofuran (4 mL) and methanol (4 mL) and the mixture heated at reflux for 20 h. Following cooling to ambient temperature, a solution of potassium *tert*-butoxide in methanol (10 mL, 0.1 M) was added affording a deep red precipitate. The precipitate was filtered under Schlenk conditions, washed with a solution of potassium *tert*-butoxide in methanol (10 mL, 0.1 M) and hexanes (10 mL) and dried under vacuum to afford **1** as a red powder (109 mg, 67 μmol, 97%). The product was transferred directly to a nitrogen filled glovebox and all further manipulations were

carried out therein. **Route B**: A Schlenk tube was charged with the bis-vinylidene complex **5(PF$_6$)$_2$** (400 mg, 0.208 mmol), KOBu^t (58.0 mg, 0.52 mmol, 2.5 equiv), and THF (20 mL). The reaction mixture was stirred at r.t. for 2 hours. The solvent was evaporated to dryness under vacuum and the crude residue was extracted with dichloromethane (2 x 10 mL). After removal of the solvent from the combined extracts under reduced pressure, the solid material was washed with pentane (10 mL) and dried in vacuo to give **1** as a red powder (340 mg, 0.208 mmol, 100% yield). ^{1}H NMR (500 MHz, CD_2Cl_2): δ = 1.42 (br s, 30H, $C_5(CH_3)_5$), 2.00 (br s, 4H, CH_2), 2.63 (br s, 4H, CH_2), 4.21 (br s, 5H, C_5H_5), 4.41 (br s, 2H, C_5H_4), 4.90 (br s, 2H, C_5H_4), 6.80–6.89 (m, 5H, C_6H_4 and C=C*H*), 7.17–7.45 (m, 36H, C_6H_4 and C_6H_5), 7.85 (br s, 8H, C_6H_5). ^{31}P NMR (202 MHz, CD_2Cl_2): δ = 99.3. FT-IR (CH_2Cl_2) ν 2201 w,sh , 2187 w (C≡C), 2046 s,br (C≡C–Fe), 1591 s cm^{-1} (C=C). Anal. Calcd For $C_{104}H_{96}P_4Fe_3$: C, 76.29; H, 5.91. Found: C, 76.67; H, 5.51. HRMS (ESI$^+$): *m*/*z* calculated for $C_{104}H_{96}P_4{}^{56}Fe_3$, 1635.43877; calculated for $C_{104}H_{97}P_4{}^{56}Fe_3$ ([M+H]$^{+\cdot}$), 1636.4466; found: 1636.4508 (0 ppm) ([M+H]$^{+\cdot}$).

FcCH=C{1,4-C≡C-C$_6$H$_4$-C≡C-Ru(dppe)Cp*}$_2$ (2). Potassium fluoride (10 mg, 175 μmol) and RuCl(dppe)Cp* (117 mg, 175 μmol) were added to a solution of **3** (53.0 mg, 88.0 μmol) in tetrahydrofuran (5 mL) and methanol (5 mL) and the mixture was heated at reflux for 16 h. After cooling to ambient temperature, methanol (15 mL) was added affording an orange precipitate. The precipitate was collected by filtration, washed with methanol (2 × 15 mL) and hexanes (2 × 15 mL) and dried under vacuum to afford **2** as an orange powder (99 mg, 57 μmol, 65%). ^{1}H NMR (600 MHz, CD_2Cl_2): δ =

1.57 (s, 15H, $C_5(CH_3)_5$), 1.58 (s, 15H, $C_5(CH_3)_5$), 2.11 (m, 4H, CH_2), 2.69 (m, 4H, CH_2), 4.20 (s, 5H, C_5H_5), 4.41 (m, 2H, C_5H_4), 4.88 (m, 2H, C_5H_4), 6.71 (m, 2H, C_6H_4), 6.76 (m, 2H, C_6H_4), 6.86 (s, 1H, C=C*H*), 7.15 (m, 2H, C_6H_4), 7.21–7.24 (m, 10H, C_6H_4 and C_6H_5), 7.37–7.39 (m, 24H, C_6H_5), 7.77 (m, 8H, C_6H_5). ^{31}P NMR (242 MHz, CD_2Cl_2): δ = 80.6. FT-IR (CH_2Cl_2 / cm^{-1}) ν(C≡C) 2189(w), ν(RuC≡C) 2062(s,br), ν(C=C) 1592 (s). MALDI-MS(+): *m/z* 1729.3 $[M+H]^+$. Anal. Calcd For $C_{104}H_{96}P_4FeRu_2$: C, 72.30; H, 5.60. Found: C, 72.15; H, 5.63.

In situ preparation of [FcCH=C{1,4-C≡C-C_6H_4-C≡C-Fe(dppe)Cp*}$_2$]$(PF_6)_n$ ($\mathbf{1(PF_6)_n}$, *n* = 0-2). A Schlenk tube was charged with **1** (0.030 g, 0.018 mmol) and THF (7 mL). The solution was cooled to -60 °C prior to adding ferrocenium hexafluorophosphate (0.0050 g, 0.018 mmol, 1 equiv) in a single portion. The temperature of the reaction mixture was allowed to reach room temperature overnight before adding 10 mL of pentane under vigorous stirring. The resulting precipitate was collected by filtration, washed with pentane (2 × 5 mL) and dried in vaccuo to yield 0.014 g of a comproportionated mixture of **1**, $\mathbf{1(PF_6)}$ and $\mathbf{1(PF_6)_2}$ as a red powder (0.0078 mmol, 40 %). For ESR measurements, the low temperature generated red solution was directly transferred via cannula into an ESR tube conserved at the liquid nitrogen temperature.

In situ generation of [FcCH=C{1,4-C≡C-C_6H_4-C≡C-Fe(dppe)Cp*}$_2$]$(PF_6)_2$ ($\mathbf{1(PF_6)_2}$). The di-oxidized product $\mathbf{1(PF_6)_2}$ was synthesized in a manner similar to that described above, from **1** (0.050 g, 0.030 mmol) and ferrocenium hexafluorophosphate

(0.020 g, 0.060 mmol, 2.0 equiv). Yield: 0.03 g (0.015 mmol, 52 %) of a red powder. The same procedure as above was carried out to prepare the ESR samples.

Computational Details. Density-functional theory (DFT) calculations were performed using the Gaussian09 program package.[79] Full geometry optimizations were carried out without any symmetry constraint using the PBE0 functional[80] within the LANL2DZ ECP basis set,[81-84] augmented by a polarization function for all atoms except H. Vibrational frequencies calculations were computed for all optimized geometries to ensure they were true minima on the potential energy surface (PES). A scaling factor of 0.95 was applied on computed vibrational frequencies discussed in the text.[85] Molecular structures, orbitals and spin densities were plotted using the GaussView program.[86] Orbital compositions were obtained using the AOMix program.[87-88]

The Amsterdam Density Functional (ADF) program.[89-91] was employed to compute the EPR properties of the cationic species using geometries optimized *via* Gaussian09. Electron correlation was treated within the local density approximation (LDA) in the Vosko−Wilk−Nusair parametrization.[92] Nonlocal corrections were added to the exchange and correlation energies using the PBE0 functional.[80] Calculations were performed using the standard ADF triple-ζ quality basis set. The ESR procedure developed by van Lenthe and co-workers was used.[93-95] The *g*-tensor components were obtained using self-consistent spin-unrestricted DFT calculations after incorporating the relativistic spin−orbit coupling by first-order perturbation theory from a ZORA Hamiltonian.[89-90]

ASSOCIATED CONTENT

- Plots of the UV-vis spectra of **1** and **2**
- Plots of the intermediate NIR spectra collected during the spectroelectrochemical oxidation of **1**
- Revised synthetic procedure for the synthesis of 4-(trimethylsilylethynyl)bromo benzene
- Plots of NMR spectra
- A MOL file of the Cartesian coordinates for all calculated geometries

NOTES

The authors declare no competing interests

ACKNOWLEDGEMENTS

The authors thank Dr. F. Gendron and Prof. Abdou Boucekkine (Rennes) for helpful discussions. Part of this work was conducted within the scope of the CNRS International Associated Laboratories “Molecular Materials and Catalysis (MMC)” (University of Durham-University of Rennes) and “Assemblages organométalliques redox-actifs et multipolaires pour la photonique et l’électronique moléculaire (REDOCHROM)” (University of Western Australia-University of Rennes). P.J.L. and J.B.G.G. thank the Australian Research Council for financial support (DP140100855).

REFERENCES

1. Natoli, S. N.; Azbell, T. J.; Fanwick, P. E.; Zeller, M.; Ren, T., A synthetic approach to cross-conjugated organometallic complexes based on geminal-diethynylethene and Co^{III}(cyclam). *Organometallics* **2016,** *35* (20), 3594-3603.
2. Forrest, W. P.; Choudhuri, M. M. R.; Kilyanek, S. M.; Natoli, S. N.; Prentice, B. M.; Fanwick, P. E.; Crutchley, R. J.; Ren, T., Synthesis and electronic structure of Ru_2(X*ap*)$_4$(Y-*gem*-DEE) type compounds: Effect of cross-conjugation. *Inorg Chem* **2015,** *54* (15), 7645-7652.
3. Xu, G. L.; Xi, B.; Updegraff, J. B.; Protasiewicz, J. D.; Ren, T., 1,6-Bis(ferrocenyl)-1,3,5-hexatriyne: Novel preparation and structural study. *Organometallics* **2006,** *25* (22), 5213-5215.
4. Bruce, M. I.; Burgun, A.; Fox, M. A.; Jevric, M.; Low, P. J.; Nicholson, B. K.; Parker, C. R.; Skelton, B. W.; White, A. H.; Zaitseva, N. N., Some Ruthenium derivatives of penta-1,4-diyn-3-one. *Organometallics* **2013,** *32* (11), 3286-3299.
5. Fan, Y.; Li, H. M.; Zou, G. D.; Zhang, X.; Li, M.; Wu, J. H.; Zhang, X.; Lu, H. T., Long-distance electronic coupling in diferrocenyl compounds with cross-conjugated geminal-diethynylethene bridges. *J Organomet Chem* **2018,** *859*, 99-105.
6. Fan, Y.; Li, H. M.; Zou, G. D.; Zhang, X.; Pan, Y. L.; Cao, K. K.; Zhang, M. L.; Ma, P. L.; Lu, H. T., Diferrocenes bridged by a geminal diethynylethene scaffold with varying pendant sSubstituents: Electronic interactions in cross-conjugated system. *Organometallics* **2017,** *36* (21), 4278-4286.
7. Gluyas, J. B. G.; Manici, V.; Guckel, S.; Vincent, K. B.; Yufit, D. S.; Howard, J. A. K.; Skelton, B. W.; Beeby, A.; Kaupp, M.; Low, P. J., Cross-conjugated systems based on an *E*-Hexa-3-en-1,5-diyne-3,4-diyl skeleton: Spectroscopic and spectroelectrochemical Investigations. *J Org Chem* **2015,** *80* (22), 11501-11512.
8. Gong, Z. L.; Zhong, Y. W.; Yao, J. N., Conformation-determined through-bond versus through-space electronic communication in mixed-valence systems with a cross-conjugated urea bridge. *Chem Eur J* **2015,** *21* (4), 1554-1566.
9. Solomon, G. C.; Andrews, D. Q.; Goldsmith, R. H.; Hansen, T.; Wasielewski, M. R.; Van Duyne, R. P.; Ratner, M. A., Quantum interference in acyclic systems: Conductance of cross-conjugated molecules. *J Am Chem Soc* **2008,** *130* (51), 17301-17308.
10. Solomon, G. C.; Andrews, D. Q.; Van Duyne, R. R.; Ratner, M. A., Electron transport through conjugated molecules: When the π system only tells part of the story. *ChemPhysChem* **2009,** *10* (1), 257-264.
11. Solomon, G. C.; Bergfield, J. P.; Stafford, C. A.; Ratner, M. A., When "small" terms matter: Coupled interference features in the transport properties of cross-conjugated molecules. *Beilstein J Nanotech* **2011,** *2*, 862-871.
12. Schafer, J.; Holzapfel, M.; Mladenova, B.; Kattnig, D.; Krummenacher, I.; Braunschweig, H.; Grampp, G.; Lambert, C., Hole transfer processes in *meta*- and *para*-conjugated mixed valence compounds: Unforeseen effects of bridge substituents and solvent dynamics. *J Am Chem Soc* **2017,** *139* (17), 6200-6209.
13. Kaliginedi, V.; Moreno-Garcia, P.; Valkenier, H.; Hong, W. J.; Garcia-Suarez, V. M.; Buiter, P.; Otten, J. L. H.; Hummelen, J. C.; Lambert, C. J.; Wandlowski, T.,

Correlations between molecular structure and single-junction conductance: A case study with oligo(phenylene-ethynylene)-type wires. *J Am Chem Soc* **2012,** *134* (11), 5262-5275.
14. Andrews, D. Q.; Solomon, G. C.; Van Duyne, R. P.; Ratner, M. A., Single molecule electronics: Increasing dynamic range and switching speed using cross-conjugated species. *J Am Chem Soc* **2008,** *130* (51), 17309-17319.
15. Lambert, C. J., Basic concepts of quantum interference and electron transport in single-molecule electronics. *Chem Soc Rev* **2015,** *44* (4), 875-888.
16. Nichols, R. J.; Higgins, S. J., Molecular Junctions: Interference comes into view. *Nat Nanotechnol* **2012,** *7* (5), 281-282.
17. Arroyo, C. R.; Tarkuc, S.; Frisenda, R.; Seldenthuis, J. S.; Woerde, C. H. M.; Eelkema, R.; Grozema, F. C.; van der Zant, H. S. J., Signatures of quantum interference effects on charge transport through a single benzene ring. *Angew Chem Int Ed* **2013,** *52* (11), 3152-3155.
18. Andrews, D. Q.; Solomon, G. C.; Goldsmith, R. H.; Hansen, T.; Wasielewski, M. R.; Van Duyne, R. P.; Ratner, M. A., Quantum interference: The structural dependence of electron transmission through model systems and cross-conjugated molecules. *J Phys Chem C* **2008,** *112* (43), 16991-16998.
19. Cardamone, D. M.; Stafford, C. A.; Mazumdar, S., Controlling quantum transport through a single molecule. *Nano Lett* **2006,** *6* (11), 2422-2426.
20. Markussen, T.; Stadler, R.; Thygesen, K. S., The relation between structure and quantum interference in single molecule junctions. *Nano Lett* **2010,** *10* (10), 4260-4265.
21. Garner, M. H.; Solomon, G. C.; Strange, M., Tuning conductance in aromatic molecules: Constructive and counteractive substituent effects. *J Phys Chem C* **2016,** *120* (17), 9097-9103.
22. Kocherzhenko, A. A.; Grozema, F. C.; Siebbeles, L. D. A., Charge transfer through molecules with multiple pathways: Quantum interference and dephasing. *J Phys Chem C* **2010,** *114* (17), 7973-7979.
23. Gorczak, N.; Renaud, N.; Galan, E.; Eelkema, R.; Siebbeles, L. D. A.; Grozema, F. C., Computational design of donor-bridge-acceptor systems exhibiting pronounced quantum interference effects. *Phys Chem Chem Phys* **2016,** *18* (9), 6773-6779.
24. Kocherzhenko, A. A.; Siebbeles, L. D. A.; Grozema, F. C., Chemically gated quantum-interference-based molecular transistor. *J Phys Chem Lett* **2011,** *2* (14), 1753-1756.
25. Launay, J. P., An orbital approach of electron transfer in multisite systems. Implications for carbon-rich spacers. *Polyhedron* **2015,** *86*, 151-166.
26. Heckmann, A.; Lambert, C., Organic mixed-valence compounds: A playground for electrons and holes. *Angew Chem Int Ed* **2012,** *51* (2), 326-392.
27. Parthey, M.; Kaupp, M., Quantum-chemical insights into mixed-valence systems: within and beyond the Robin-Day scheme. *Chem Soc Rev* **2014,** *43* (14), 5067-5088.
28. Brunschwig, B. S.; Creutz, C.; Sutin, N., Optical transitions of symmetrical mixed-valence systems in the Class II-III transition regime. *Chem Soc Rev* **2002,** *31* (3), 168-184.

29. Brunschwig, B. S.; Sutin, N., Energy surfaces, reorganization energies, and coupling elements in electron transfer. *Coord Chem Rev* **1999,** *187*, 233-254.
30. Launay, J. P., Electron transfer in molecular binuclear complexes and relation with electron transport through nanojunctions. *Coord Chem Rev* **2013,** *257* (9-10), 1544-1554.
31. Vincent, K. B.; Zeng, Q.; Parthey, M.; Yufit, D. S.; Howard, J. A. K.; Hartl, F.; Kaupp, M.; Low, P. J., Syntheses, spectroelectrochemical studies, and molecular and electronic structures of ferrocenyl ene-diynes. *Organometallics* **2013,** *32* (20), 6022-6032.
32. Vincent, K. B.; Gluyas, J. B. G.; Zeng, Q.; Yufit, D. S.; Howard, J. A. K.; Hartl, F.; Low, P. J., Sandwich and half-sandwich metal complexes derived from cross-conjugated 3-methylene-penta-1,4-diynes. *Dalton Trans* **2017,** *46* (17), 5522-5531.
33. Vincent, K. B.; Gluyas, J. B. G.; Guckel, S.; Zeng, Q.; Hartl, F.; Kaupp, M.; Low, P. J., Tetrakis(ferrocenylethynyl)ethene: Synthesis, (spectro)electrochemical and quantum chemical characterisation. *J Organomet Chem* **2016,** *821*, 40-47.
34. Halet, J. F.; Lapinte, C., Charge delocalization vs localization in carbon-rich iron mixed-valence complexes: A subtle interplay between the carbon spacer and the (dppe)Cp*Fe organometallic electrophore. *Coord Chem Rev* **2013,** *257* (9-10), 1584-1613.
35. Bruce, M. I.; Low, P. J., Transition metal complexes containing all-carbon ligands. *Adv Organomet Chem* **2004,** *50*, 179-444.
36. Low, P. J.; Bruce, M. I., Transition metal chemistry of 1,3-diynes, poly-ynes, and related compounds. *Adv Organomet Chem* **2001,** *48*, 71-288.
37. Guckel, S.; Gluyas, J. B. G.; El-Tarhuni, S.; Sobolev, A. N.; Whiteley, M. W.; Halet, J. F.; Lapinte, C.; Kaupp, M.; Low, P. J., Iron versus Ruthenium: Clarifying the electronic differences between prototypical mixed-valence organometallic butadiyndiyl bridged molecular wires. *Organometallics* **2018,** *37* (9), 1432-1445.
38. Gluyas, J. B. G.; Guckel, S.; Kaupp, M.; Low, P. J., Rational control of conformational distributions and mixed-valence characteristics in diruthenium complexes. *Chem-Eur J* **2016,** *22* (45), 16138-16146.
39. Parthey, M.; Gluyas, J. B. G.; Fox, M. A.; Low, P. J.; Kaupp, M., Mixed-valence Ruthenium complexes rotating through a conformational Robin-Day continuum. *Chem Eur J* **2014,** *20* (23), 6895-6908.
40. Parthey, M.; Gluyas, J. B. G.; Schauer, P. A.; Yufit, D. S.; Howard, J. A. K.; Kaupp, M.; Low, P. J., Refining the interpretation of Near-Infrared Band shapes in a polyynediyl molecular wire. *Chem Eur J* **2013,** *19* (30), 9780-9784.
41. Paul, F.; Lapinte, C., Organometallic molecular wires and other nanoscale-sized devices. An approach using the organoiron (dppe)Cp*Fe building block. *Coord Chem Rev* **1998,** *178*, 431-509.
42. Bruce, M. I.; Wallis, R. C., Cyclopentadienyl-Ruthenium and cyclopentadienyl-Osmium chemistry 9. Some substituted η^1-vinylidene and η^1-acetylide complexes. *Aust J Chem* **1979,** *32* (7), 1471-1485.
43. Bruce, M. I., Organometallic chemistry of vinylidene and related unsaturated carbenes. *Chem Rev* **1991,** *91* (2), 197-257.

44. Gluyas, J. B. G.; Brown, N. J.; Farmer, J. D.; Low, P. J., Optimised syntheses of the half-sandwich complexes FeCl(dppe)Cp*, FeCl(dppe)Cp, RuCl(dppe)Cp*, and RuCl(dppe)Cp. *Aust J Chem* **2017,** *70* (1), 113-119.
45. Connelly, N. G.; Gamasa, M. P.; Gimeno, J.; Lapinte, C.; Lastra, E.; Maher, J. P.; Le Narvor, N.; Rieger, A. L.; Rieger, P. H., 17-Electron Alkynyl Complexes of Cyclopentadienyliron(III). *J Chem Soc Dalton Trans* **1993,** (17), 2575-2578.
46. Le Narvor, N.; Lapinte, C., 1,4-Diethynylbenzene bridged Fe(Cp*)(dppe) units - Mixed-valence 35-electron and bisiron(III) 34-electron complexes. *Organometallics* **1995,** *14* (2), 634-639.
47. Bruce, M. I.; Hameister, C.; Swincer, A. G.; Wallis, R. C., Some "η^5-Cyclopentadienylruthenium(II) complexes containing triphenylphosphine. *Inorg Synth* **1982,** *21*, 78-84.
48. Bruce, M. I.; Hall, B. C.; Kelly, B. D.; Low, P. J.; Skelton, B. W.; White, A. H., An efficient synthesis of polyynyl and polyynediyl complexes of ruthenium(II). *J Chem Soc Dalton Trans* **1999,** (21), 3719-3728.
49. Bruce, M. I.; Low, P. J.; Hartl, F.; Humphrey, P. A.; de Montigny, F.; Jevric, M.; Lapinte, C.; Perkins, G. J.; Roberts, R. L.; Skelton, B. W.; White, A. H., Syntheses, structures, some reactions, and electrochemical oxidation of ferrocenylethynyl complexes of iron, ruthenium, and osmium. *Organometallics* **2005,** *24* (22), 5241-5255.
50. Burgun, A.; Gendron, F.; Sumby, C. J.; Roisnel, T.; Cador, O.; Costuas, K.; Halet, J. F.; Bruce, M. I.; Lapinte, C., Hexatriynediyl chain spanning two Cp*(dppe)M termini (M = Fe, Ru): Evidence for the dependence of electronic and magnetic couplings on the relative orientation of the termini. *Organometallics* **2014,** *33* (10), 2613-2627.
51. Akita, M.; Tanaka, Y.; Naitoh, C.; Ozawa, T.; Hayashi, N.; Takeshita, M.; Inagaki, A.; Chung, M. C., Synthesis of a series of diiron complexes based on a tetraethynylethene skeleton and related C_6-enediyne spacers, (dppe)Cp*Fe-C≡CC(R)=C(R)=C≡C-FeCp*(dppe): Tunable molecular wires. *Organometallics* **2006,** *25* (22), 5261-5275.
52. Fox, M. A.; Roberts, R. L.; Baines, T. E.; Le Guennic, B.; Halet, J. F.; Hartl, F.; Yufit, D. S.; Albesa-Jove, D.; Howard, J. A. K.; Low, P. J., Ruthenium complexes of C,C'-bis(ethynyl)carboranes: An investigation of electronic interactions mediated by spherical pseudo-aromatic spacers. *J Am Chem Soc* **2008,** *130* (11), 3566-3578.
53. Gendron, F.; Burgun, A.; Skelton, B. W.; White, A. H.; Roisnel, T.; Bruce, M. I.; Halet, J. F.; Lapinte, C.; Costuas, K., Iron and Ruthenium σ-polyynyls of the general formula $[\{M(dppe)Cp^*\}-(C\equiv C)_n-R]^{0/+}$ (M = Fe, Ru): An experimental and theoretical investigation. *Organometallics* **2012,** *31* (19), 6796-6811.
54. Armitt, D. J.; Bruce, M. I.; Gaudio, M.; Zaitseva, N. N.; Skelton, B. W.; White, A. H.; Le Guennic, B.; Halet, J. F.; Fox, M. A.; Roberts, R. L.; Hartl, F.; Low, P. J., Some transition metal complexes derived from mono- and di-ethynyl perfluorobenzenes. *Dalton Trans* **2008,** (47), 6763-6775.
55. Denis, R.; Toupet, L.; Paul, F.; Lapinte, C., Electron-rich piano-stool iron σ-acetylides bearing a functional aryl group. Synthesis and characterization of iron(II) and iron(III) complexes. *Organometallics* **2000,** *19* (21), 4240-4251.

56. Paul, F.; Ellis, B. G.; Bruce, M. I.; Toupet, L.; Roisnel, T.; Costuas, K.; Halet, J. F.; Lapinte, C., Bonding and substituent effects in electron-rich mononuclear ruthenium σ-arylacetylides of the formula $[(\eta^2\text{-dppe})(\eta^5\text{-}C_5Me_5)Ru(C{\equiv}C)\text{-}1,4\text{-}(C_6H_4)X][PF_6]_n$ (n = 0, 1; X = NO_2, CN, F, H, OMe, NH_2). *Organometallics* **2006,** *25* (3), 649-665.
57. Connelly, N. G.; Geiger, W. E., Chemical redox agents for organometallic chemistry. *Chem Rev* **1996,** *96* (2), 877-910.
58. Paul, F.; Toupet, L.; Thepot, J. Y.; Costuas, K.; Halet, J. F.; Lapinte, C., Electron-rich piano-stool iron sigma-acetylides. Electronic structures of arylalkynyl iron(III) radical cations. *Organometallics* **2005,** *24* (22), 5464-5478.
59. Sato, M.; Hayashi, Y.; Shintate, H.; Katada, M.; Kawata, S., Oxidized FeII ferrocenylacetylide complexes - A novel type of mixed-valence complex. *J Organomet Chem* **1994,** *471* (1-2), 179-184.
60. Sato, M.; Hayashi, Y.; Kumakura, S.; Shimizu, N.; Katada, M.; Kawata, S., Synthesis and oxidation of iron(II) ferrocenylacetylide diphosphine complexes. A novel type of mixed-valence complex. *Organometallics* **1996,** *15* (2), 721-728.
61. Costuas, K.; Paul, F.; Toupet, L.; Halet, J. F. O.; Lapinte, C., Electron-rich piano-stool iron σ-acetylides. Theoretical and phenomenological investigation of electronic substituent effects in iron(II) acetylides. *Organometallics* **2004,** *23* (9), 2053-2068.
62. Fox, M. A.; Roberts, R. L.; Khairul, W. M.; Hartl, F.; Low, P. J., Spectroscopic properties and electronic structures of 17-electron half-sandwich ruthenium acetylide complexes, $[Ru(CCAr)(L_2)Cp']^+$ (Ar = phenyl, *p*-tolyl, 1-naphthyl, 9-anthryl; $L_2 = (PPh_3)_2$, Cp' = Cp; L_2 = dppe; Cp' = Cp*). *J Organomet Chem* **2007,** *692* (15), 3277-3290.
63. Fox, M. A.; Farmer, J. D.; Roberts, R. L.; Humphrey, M. G.; Low, P. J., Noninnocent ligand behavior in diruthenium complexes containing a 1,3-diethynylbenzene bridge. *Organometallics* **2009,** *28* (17), 5266-5269.
64. Lohan, M.; Justaud, F.; Lang, H.; Lapinte, C., Synthesis, spectroelectrochemical, and EPR spectroscopic studies of mixed bis(alkynyl)biferrocenes of the type $(L_nMC{\equiv}C)(L_nM'C{\equiv}C)$bfc. *Organometallics* **2012,** *31* (9), 3565-3574.
65. Loban, M.; Ecorchard, P.; Ruffer, T.; Justaud, F.; Lapinte, C.; Lang, H., 1',1'''-Bis(ethynyl)biferrocene as a linking group for Gold, Ruthenium, and Osmium fragments: Synthesis, solid state structures, and electrochemical, UV-Vis, and EPR spectroscopical studies. *Organometallics* **2009,** *28* (6), 1878-1890.
66. Cao, Z.; Ren, T., DFT study of electronic properties of 3d metal complexes of σ-geminal diethynylethenes (*gem*-DEEs). *Organometallics* **2011,** *30* (2), 245-250.
67. Bruschi, M.; Giuffreda, M. G.; Luthi, H. P., Through versus cross electron delocalization in polytriacetylene oligomers: A computational analysis. *ChemPhysChem* **2005,** *6* (3), 511-519.
68. Bruschi, M.; Giuffreda, M. G.; Luthi, H. P., *trans* versus *geminal* electron delocalization in tetra- and diethynylethenes: A new method of analysis. *Chem Eur J* **2002,** *8* (18), 4216-4227.
69. Bruce, M. I.; Ellis, B. G.; Low, P. J.; Skelton, B. W.; White, A. H., Syntheses, structures, and spectro-electrochemistry of {Cp*(PP)Ru}C≡CC≡C{Ru(PP)Cp*}

(PP = dppm, dppe) and their mono- and dicationst. *Organometallics* **2003,** *22* (16), 3184-3198.
70. Seiler, P.; Dunitz, J. D., Structure of triclinic ferrocene at 101-K, 123-K and 148-K. *Acta Crystallogr B* **1979,** *35* (Sep), 2020-2032.
71. Gauthier, N.; Tchouar, N.; Justaud, F.; Argouarch, G.; Cifuentes, M. P.; Toupet, L.; Touchard, D.; Halet, J. F.; Rigaut, S.; Humphrey, M. G.; Costuas, K.; Paul, F., Bonding and electron delocalization in Ruthenium(III) σ-arylacetylide radicals [*trans*-Cl(η^2-dppe)$_2$RuC≡C(4-C_6H_4X)]$^+$ (X = NO_2, C(O)H, C(O)Me, F, H, OMe, NMe_2): Misleading Aspects of the ESR Anisotropy. *Organometallics* **2009,** *28* (7), 2253-2266.
72. Eischenbroich, C.; Bilger, E.; Ernst, R. D.; Wilson, D. R.; Kralik, M. S., Closed, half-open, and open ferrocenes - Redox behavior and Electron-Spin Resonance of the radical cations. *Organometallics* **1985,** *4* (11), 2068-2071.
73. Sixt, T.; Fiedler, J.; Kaim, W., Iron versus ruthenium oxidation in 1,1'-bis(diphenylphosphino)ferrocene-ruthenium(II) complexes: EPR and spectroelectrochemical evidence. *Inorg Chem Commun* **2000,** *3* (2), 80-82.
74. Kramer, J. A.; Hendrickson, D. N., Electron-transfer in mixed-valent diferrocenylacetylene and [2.2]ferrocenophane-1,13-diyne. *Inorg Chem* **1980,** *19* (11), 3330-3337.
75. Coulson, D. R.; Satek, L. C.; Grim, S. O., Tetrakis(triphenylphosphine)Palladium(0). *Inorg Synth* **1990,** *28*, 107-109.
76. Marques-Gonzalez, S.; Parthey, M.; Yufit, D. S.; Howard, J. A. K.; Kaupp, M.; Low, P. J., Combined spectroscopic and quantum chemical study of [*trans*-Ru(C≡$C_6H_4R^1$-4)$_2$(dppe)$_2$]$^{n+}$ and [*trans*-Ru(C≡$CC_6H_4R^1$-4)(C≡$CC_6H_4R^2$-4)(dppe)$_2$]$^{n+}$ (n = 0, 1) complexes: Interpretations beyond the lowest energy conformer paradigm. *Organometallics* **2014,** *33* (18), 4947-4963.
77. Fulmer, G. R.; Miller, A. J. M.; Sherden, N. H.; Gottlieb, H. E.; Nudelman, A.; Stoltz, B. M.; Bercaw, J. E.; Goldberg, K. I., NMR chemical shifts of trace impurities: Common laboratory solvents, organics, and gases in deuterated solvents relevant to the Organometallic Chemist. *Organometallics* **2010,** *29* (9), 2176-2179.
78. Krejcik, M.; Danek, M.; Hartl, F., Simple construction of an Infrared Optically Transparent Thin-Layer Electrochemical-cell - Applications to the redox reactions of Ferrocene, $Mn_2(CO)_{10}$ and $Mn(CO)_3$(3,5-di-t-butyl-catecholate)$^-$. *J Electroanal Chem* **1991,** *317* (1-2), 179-187.
79. Frisch, M. J.; Trucks, G. W.; Schlegel, H. B.; Scuseria, G. E.; Robb, M. A.; Cheeseman, J. R.; Scalmani, G.; Barone, V.; Menucci, B.; Petersson, G. A.; Nakatsuji, H.; Caricato, M.; Hratchian, X.; Li, H. P.; Izmaylov, A. F.; Bloino, J.; Zheng, G.; Sonnenberg, J. L.; Hada, M.; Ehara, M.; Toyota, K.; Fukuda, R.; Hasegawa, J.; Ishida, M.; Nakajima, T.; Honda, Y.; Kitao, O.; Nakai, H.; Vreven, T.; Montgomery, J. A. J.; Peralta, J. E.; Ogliaro, F.; Bearpark, M.; Heyd, J. J.; Brothers, E.; Kudin, K. N.; Staroverov, V. N.; Keith, T.; Kobayashi, R.; Normand, J.; Raghavchari, K.; Rendell, A.; Burant, J. C.; Iyenfar, S. S.; Tomasi, J.; Cossi, M.; Rega, N.; Millam, J. M.; Klene, M.; Knox, J. E.; Cross, J. B.; Bakken, V.; Adamo, C.; Jaramillo, J.; Gomperts, R.; Stratmann, R. E.; Yazyev, O.; Austin, A. J.; Cammi, R.; Pomelli, C.; Ochterski, J. W.; Martin, R. L.; Morokuma, K.; Zakrzewski, V. G.; Voth, G. A.; Salvador, P.; Dannenberg, J. J.; Dapprich, S.;

Daniels, A. D.; Farkas, O.; Foresman, J. B.; Oritz, J. V.; Cioslowski, J.; Fox, D. J. *Gaussian09*, Revision A.02; Gaussian Inc, Wallingford, CT: 2009.
80. Vetere, V.; Adamo, C.; Maldivi, P., Performance of the 'parameter free' PBE0 functional for the modeling of molecular properties of heavy metals. *Chem Phys Lett* **2000,** *325* (1-3), 99-105.
81. Dunning, T. H. J.; Hay, P. J., *Methods of Electronic Structure Theory*. Plenum: New York, 1976; Vol. 3.
82. Wadt, W. R.; Hay, P. J., Ab initio effective core potentials for molecular calculations - Potentials for main group elements Na to Bi. *J Chem Phys* **1985,** *82* (1), 284-298.
83. Hay, P. J.; Wadt, W. R., Ab initio effective core potentials for molecular calculations - Potentials for K to Au including the outermost core orbitals. *J Chem Phys* **1985,** *82* (1), 299-310.
84. Hay, P. J.; Wadt, W. R., Ab initio effective core potentials for molecular calculations - Potentials for the transition-metal atoms Sc to Hg. *J Chem Phys* **1985,** *82* (1), 270-283.
85. Yu, L.; Srinivas, G. N.; Schwartz, M., Scale factors for C=O vibrational frequencies in organometallic complexes. *J Mol Struc-Theochem* **2003,** *625*, 215-220.
86. Dennington, R.; Keith, T.; Millam, J. *GaussView*, Version 5; Semichem Inc, Shawnee Mission, KS: 2009.
87. Gorelsky, S. I. *AOMix: Program for Molecular Orbital Analysis*, http://www.sg-chem.net; University of Ottawa: 2007.
88. Gorelsky, S. I.; Lever, A. B. P., Electronic structure and spectral, of ruthenium diimine complexes by density functional theory and INDO/S. Comparison of the two methods. *J Organomet Chem* **2001,** *635* (1-2), 187-196.
89. te Velde, G.; Bickelhaupt, F. M.; Baerends, E. J.; Guerra, C. F.; Van Gisbergen, S. J. A.; Snijders, J. G.; Ziegler, T., Chemistry with ADF. *J Comput Chem* **2001,** *22* (9), 931-967.
90. Guerra, C. F.; Snijders, J. G.; te Velde, G.; Baerends, E. J., Towards an order-N DFT method. *Theor Chem Acc* **1998,** *99* (6), 391-403.
91. *ADF2010.02, SCM*, Theoretical Chemistry, Vrije Universiteit: Amsterdam, The Netherlands, http://www.scm.com.
92. Vosko, S. H.; Wilk, L.; Nusair, M., Accurate spin-dependent electron liquid correlation energies for local spin-density calculations - A critical analysis. *Can J Phys* **1980,** *58* (8), 1200-1211.
93. van Lenthe, E.; van der Avoird, A.; Wormer, P. E. S., Density functional calculations of molecular hyperfine interactions in the zero order regular approximation for relativistic effects. *J Chem Phys* **1998,** *108* (12), 4783-4796.
94. vanLenthe, E.; Wormer, P. E. S.; vanderAvoird, A., Density functional calculations of molecular *g*-tensors in the zero-order regular approximation for relativistic effects. *J Chem Phys* **1997,** *107* (7), 2488-2498.
95. Autschbach, J.; Pritchard, B., Calculation of molecular *g*-tensors using the zeroth-order regular approximation and density functional theory: expectation value versus linear response approaches. *Theor Chem Acc* **2011,** *129* (3-5), 453-466.